NAVAL POSTGRADUATE SCHOOL
Monterey, California

DTIC QUALITY INSPECTED 4

THESIS

LINE BROADENING ANALYSIS
OF
MPD THRUSTERS

by

William A. Bullard, III

March, 1997

Thesis Advisor: David Cleary
Co-Advisor: Oscar Biblarz

Approved for public release; distribution is unlimited.

19970828 063

REPORT DOCUMENTATION PAGE

Form Approved OMB No. 0704-0188

1. AGENCY USE ONLY *(Leave blank)*	2. REPORT DATE March 1997	3. REPORT TYPE AND DATES COVERED Master's Thesis

4. TITLE AND SUBTITLE LINE BROADENING ANALYSIS OF MPD THRUSTERS	5. FUNDING NUMBERS
6. AUTHOR(S) William A. Bullard III	

7. PERFORMING ORGANIZATION NAME(S) AND ADDRESS(ES) Naval Postgraduate School Monterey CA 93943-5000	8. PERFORMING ORGANIZATION REPORT NUMBER

9. SPONSORING/MONITORING AGENCY NAME(S) AND ADDRESS(ES) NASA Jet Propulsion Laboratory Pasadena, CA	10. SPONSORING/MONITORING AGENCY REPORT NUMBER

11. SUPPLEMENTARY NOTES The views expressed in this thesis are those of the author and do not reflect the official policy or position of the Department of Defense or the U.S. Government.

12a. DISTRIBUTION/AVAILABILITY STATEMENT Approved for public release; distribution is unlimited.	12b. DISTRIBUTION CODE

13. ABSTRACT *(maximum 200 words)*

Spectroscopic analysis of the cathode jet of a model coaxial magneto-plasma dynamic (MPD) thruster is conducted to determine electron density and temperature downstream from the cathode. H_β line profiles were scanned from an argon-hydrogen plasma generated in the cathode test facility of the NASA Jet Propulsion Laboratory in Pasadena, CA. A computer program was written in IDL to determine the profile Doppler- and Stark half widths, which were used to determine temperature and electron density, respectively. Three sets of data from the cathode test facility were taken, while varying operating voltage, current, hydrogen/argon ratio, and pressure. Radial profiles for electron density and temperature were determined within the cathode jet. Generated plasmas ranged in electron density and temperature from approximately $N_e = 2\times10^{14}$ cm^{-3} at 5000 K (0.43 eV) to 4×10^{14} cm^{-3} at 15600 K (1.3 eV). It was determined that radial density and temperature distribution within the cathode jet are essentially uniform.

14. SUBJECT TERMS Electromagnetic propulsion, Doppler broadening, Stark broadening, Plasma spectroscopy			15. NUMBER OF PAGES 102
			16. PRICE CODE

17. SECURITY CLASSIFICATION OF REPORT Unclassified	18. SECURITY CLASSIFICATION OF THIS PAGE Unclassified	19. SECURITY CLASSIFICATION OF ABSTRACT Unclassified	20. LIMITATION OF ABSTRACT UL

NSN 7540-01-280-5500

Standard Form 298 (Rev. 2-89)
Prescribed by ANSI Std. 239-18 298-102

LINE BROADENING ANALYSIS
OF
MPD THRUSTERS

William A. Bullard, III
Lieutenant, United States Navy
B.S., Worcester Polytechnic Institute, 1990

Submitted in partial fulfillment
of the requirements for the degree of

MASTER OF SCIENCE IN APPLIED PHYSICS
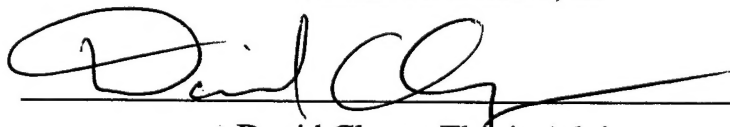
from the

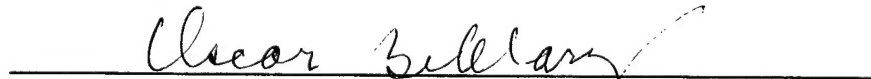## NAVAL POSTGRADUATE SCHOOL
March 1997

Author: _____

William A. Bullard, III

Approved by: _____

David Cleary, Thesis Advisor

_____

Oscar Biblarz, Co-Advisor

_____

Anthony Atchley, Chairman Department of Physics

iii

ABSTRACT

Spectroscopic analysis of the cathode jet of a model coaxial magneto-plasma dynamic (MPD) thruster is conducted to determine electron density and temperature downstream from the cathode. H_β line profiles were scanned from an argon-hydrogen plasma generated in the cathode test facility of the NASA Jet Propulsion Laboratory in Pasadena, CA. A computer program was written in IDL to determine the profile Doppler- and Stark half widths, which were used to determine temperature and electron density, respectively. Three sets of data from the cathode test facility were taken, while varying operating voltage, current, hydrogen/argon ratio, and pressure. Radial profiles for electron density and temperature were determined within the cathode jet. Generated plasmas ranged in electron density and temperature from approximately $N_e = 2\times10^{14}$ cm^{-3} at 5000 K (0.43 eV) to 4×10^{14} cm^{-3} at 15600 K (1.3 eV). It was determined that radial density and temperature distribution within the cathode jet are essentially uniform.

TABLE OF CONTENTS

LIST OF FIGURES

x

LIST OF TABLES

ACKNOWLEDGMENT

I wish to thank several people whose support greatly aided in the completion of this work. Thanks to Professor Cleary and Professor Biblarz, for allowing me to follow my own road on this journey. To Drs. John Brophy, Keith Goodfellow, and Jay Polk of the Advanced Propulsion Technology Group at NASA Jet Propulsion Laboratory, for having patience with a neophyte, making me feel at home, buying me pizza, and showing me the future of space propulsion.

To Jessie Fisher and Kathy Nyberg, who were good enough to put up with me as a roommate during my stay at JPL. To Lori McKinney, who always had faith and encouraging words for me, even at the height of stress and frustration. And finally, to Sarah Johnston, because of the way you make me smile.

I. INTRODUCTION

A.   THESIS OBJECTIVES

The objective of this thesis is to develop a method for estimating electron densities and temperatures in the plasma jet of a model magnetoplasma-dynamic thruster, such as those presently in development for space propulsion, by analyzing the broadening of spectral emissions within the plasma. Both Doppler and Stark broadening effects are analyzed to respectively determine a radial temperature and electron density profile within the plasma arc. A computer program was written to analyze the broadening of hydrogen line profiles by unfolding and examining the Stark and Doppler half widths of the line profile. Three sets of data taken at the NASA Jet Propulsion Laboratory (JPL) Cathode Test Facility (CTF) are analyzed.

B.   THESIS OUTLINE

This thesis is divided into six chapters and three appendices, describing the background, conduct, data analysis and conclusions of the experiment. Chapter II provides background information for the thesis, giving a brief overview of the basic concepts of plasmas, magnetoplasma-dynamic thrusters, and the theory of atomic radiation. Chapter III continues the background discussion, outlining Doppler broadening, the Stark effect and Stark broadening, and line broadening analysis of spectral lines. Chapter IV describes the experimental facility at NASA JPL, as well as the data collection process. Chapter V describes the computer program written to analyze the data gathered, and presents and discusses the analysis of the three data sets. Chapter VI presents conclusions and discussion for the furthering and improvement of this and like experiments.

Appendix A is the listing of the computer program, written in Interactive Data Language (IDL), which was written to analyze the data collected. Appendix B presents the results of the experiment and analysis in tabular form. Appendix C contains data tables used for the interpolations in the IDL program.

II. BACKGROUND

A.   ELECTRIC PROPULSION DEFINITION

Electric propulsion may be defined as the acceleration of gases for propulsion by electrical heating and/ or by electric and magnetic body forces. As is evident in the definition, electric propulsion may be subdivided into three distinct categories: (Jahn, 1968)

> 1. *Electrothermal.* Propellant is electrically heated and thermodynamically expanded and accelerated to supersonic speeds through a nozzle, as in a chemical rocket.

> 2. *Electrostatic.* Propellant is accelerated by the interaction of electrostatic fields on charged particles, such as ions or colloids.

> 3. *Electromagnetic.* Acceleration is achieved through the interaction of electric and magnetic fields on a highly ionized propellant gas.

1.   Plasma Thrusters

Specifically, electromagnetic propulsion deals with the acceleration of a plasma, a highly ionized quasi-neutral gas, through the interaction of currents driven through the gas with magnetic fields established either by those currents or by external means (Jahn, 1968). Numerous ways exist of classifying electromagnetic thrusters, from thrust mode to working fluid path geometry, and the names for these various thrusters are equally as varied. The work performed for this thesis applies to a developmental facility for a *steady-state, coaxial, magnetoplasma-dynamic* (MPD) *thruster.*

a.   The Coaxial MPD Thruster

A basic diagram of a coaxial MPD thruster, showing its operation, is shown in Figure 2.1 on the following page. A propellant gas, commonly hydrogen, argon or xenon, is fed into the cylindrical thrust chamber and is ionized. Current is driven through the plasma by an external power supply connected across the concentric anode and cathode. The induction of a magnetic field by the axial current component, or

3

the application of a magnetic field externally, accelerates the propellant by the resulting $(j \times B)$ force.

Several models of plasma thrusters, both pulsed and steady state, have been flown on satellites by the United States and the former USSR for station keeping and orbit mainetenance purposes (Sutton, 1992). However, MPD thrusters may have benefits reaching far beyond their limited application to date. Their high exhaust velocities and specific impulse make them appealing candidates for long duration, high impulse space missions, such as planetary transfers and deep space probes.
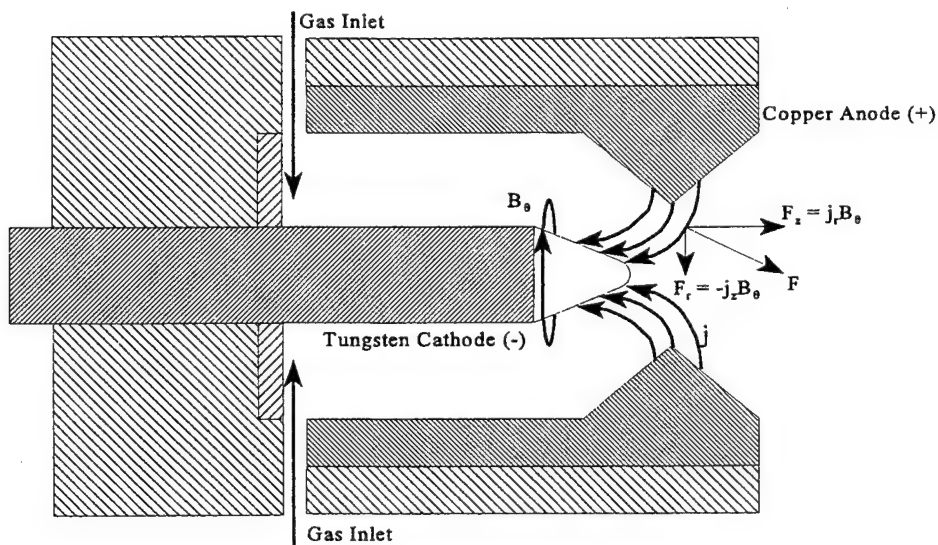
Figure 2.1. MPD Thruster Operation

While some models of plasma thrusters have been flown, electromagnetic propulsion is still a largely developmental discipline. MPD thrusters employ both electromagnetic and plasma phenomena, both of which can prove very difficult to analytically model. Additionally, current designs are relatively inefficient, and large plasma thrusters for long duration missions have very high power requirements. (Sutton, 1992)

B.   PLASMA DEFINITION AND PARAMETERS

Plasma, the most abundant state of matter in the universe, can be simply described as an electrified gas with atoms dissociated into positive (ions) and negative (electrons) charged particles. The degree of ionization for such a gas at thermal equilibrium is determined by the Saha equation:

$$\frac{n_i}{n_n} = 2.4 \times 10^{15} \frac{T^{3/2}}{n_i} \, e^{-U_i/kT} \qquad (2.1)$$

Here, n_i and n_n are, respectively, the number density (per cubic centimeter) of ionized and neutral atoms, T is the gas temperature in K, k is Boltzmann's constant, and U_i is the ionization energy of the gas in question.

Although all gases have some degree of ionization, not all gases may be referred to as plasmas. A more specific definition of a plasma is *a quasineutral gas of charged and neutral particles that exhibits collective behavior* (Chen, 1974).

1.   Plasma Temperature

At thermal equilibrium, a gas has a distribution of velocities and, therefore, kinetic energies. Particle velocities most often obey a Maxwellian or Gaussian distribution. In one dimension, the velocity distribution is written as:

$$f(u)\,du = \frac{n}{v_{th}} e^{-u^2/v_{th}^2} \, du \qquad (2.2)$$

where

$$v_{th} = \sqrt{\frac{2kT}{m}} \qquad (2.3)$$

5

Here, $f(u)du$ is the number of particles (per cubic centimeter) with velocities between u and $u+du$, and v_{th} is the thermal velocity of the particle, dependent upon the temperature, T, and mass, m of the particle.

The average kinetic energy of the particles in the gas is:

$$E_{av} = \frac{1}{2} kT \qquad (2.4)$$

or, in the three dimensional case:

$$E_{av} = \frac{3}{2} kT \qquad (2.5)$$

Equations 2.4 and 2.5 show the most meaningful representation of temperature as it applies to plasmas, as a measure of average energy. Although temperature may be expressed in Kelvin, when dealing with plasmas it is common to express temperature in terms of energy, or electron volts (eV). Specifically, a 1 eV plasma means $kT = 1.6 \times 10^{-19}$ Joules = 1 eV. Therefore, a 1 eV plasma has an $E_{av} = 1.5$ eV in three dimensions.

2.   Debye Length and Sheaths

The requirement for quasineutrality in a plasma implies that the bulk of the plasma be kept free of large electric potentials or fields. This is accomplished through a process known as Debye shielding, by which plasmas "shield out" applied electric potentials.

The presence of a large potential inside a plasma would almost immediately cause a cloud of oppositely charged particles to surround the potential surface. This cloud of charged particles is known as a sheath, and it is the presence of this sheath that shields out the large potential that caused its formation. In a hypothetical plasma with no thermal motion ($kT = 0$) the total charge in the sheath would equal the total charge in the potential, and no potential would exist outside the sheath. However, in a plasma of temperature T, shielding will be imperfect. At the edge of the sheath, the energy of the electric potential is approximately equal to the thermal energy kT of the particles, which

6

could escape from the potential well, allowing potentials on the order of kT/e to exist within the plasma.

A measure of the thickness of this sheath, the Debye length, is defined as

$$\lambda_D = \sqrt{\frac{kT_e}{4\pi ne^2}} \qquad (2.6)$$

and is the distance at which the shielded potential drops by a factor of $1/e$. Accordingly, in a collisionless plasma, the field strength as a function of distance from the potential is expressed as:

$$\phi = \phi_0 \, e^{-x/\lambda_D} \qquad (2.7)$$

Note that T_e is used in defining the Debye length, as the electrons in the plasma, being in general much more mobile than the ions, do most of the shielding by creating either a surplus or deficit of negative charge.

The term quasineutrality can now be defined. In order to be considered quasi-neutral, the effects of local concentrations of charge or the introduction of external potentials into the system must be shielded out in a distance short compared to the overall dimensions of the gas. Doing so leaves the bulk of the plasma free of large electric fields and potentials. Therefore, in order for a gas to be considered a plasma, $\lambda_D << L$, where L is a measure of the size of the plasma. Furthermore, quasineutrality implies that one can take $n_e \cong n_i \cong n$. That is, n_i and n_e are considered equal, and a common density, n, called the plasma density, is used.

3.   Plasma Parameter

In order for Debye shielding to be effective there must be a sufficient number of particles inside the sheath. The number of particles in a "Debye sphere" of radius λ_D can be expressed as:

$$N_D = \frac{4}{3}\pi n \lambda_D^3 \tag{2.8}$$

For an ionized gas to be considered a plasma,

$$N_D \gg 1 \tag{2.9}$$

4.   Collision Frequency

In order for an ionized gas to behave as a plasma, the motion of charged particles within the plasma must be controlled by electromagnetic, rather than hydrodynamic, forces. All plasmas have a fundamental plasma frequency, expressed as

$$\omega_p = \sqrt{\frac{4\pi n e^2}{m}} \tag{2.10}$$

which describes the oscillation frequency of electrons inside the plasma. If τ_c is the mean time between collisions of charged particles with neutral atoms, it is required that

$$\omega_p \tau_c > 1 \tag{2.11}$$

in order for an ionized gas to behave as a plasma rather than a neutral gas.

C.   MPD PLASMA ARC

Generating and sustaining the plasma arc in an MPD thruster entails the ionizing of the propellant gas as well as establishing the current and magnetic field necessary to accelerate the plasma jet to velocities high enough to generate sufficient thrust. The

propellant gas, when injected into the thruster, is immediately exposed to an ionizing potential, existing between the cathode and the anode. The plasma is then accelerated past the nozzle-shaped anode.

1. Plasma Arc Description

In steady state operation, the plasma is readily recognizable as an intensely luminous column of gas extending from the cathode tip, called the cathode jet. Viewed externally, the exhaust plume may have a coaxial structure, consisting of the cathode jet and a less intense coaxial shell extending from the lip of the anode orifice (anode jet), separated by an even less intense region. The whole plume usually extends many anode diameters downstream (Jahn, 1968). Figure 2.2 shows a photograph of an MPD arc in vacuum tank operation. The cathode and anode jets are easily distinguishable exiting the anode orifice.
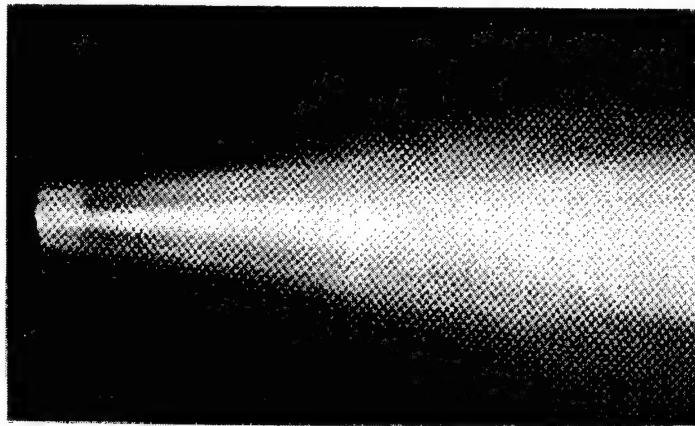
Figure 2.2. MPD Thruster Exhaust Plume (Jahn, 1968)

D. ATOMIC STRUCTURE AND RADIATION

The light emitted by the plasma arc described above, and indeed in all plasmas subjected to electrical discharges, is limited to certain discrete wavelengths that are characteristic of the gases that compose the plasma. Light emission from an atom occurs when an electron within the atom changes, or "transitions" from an initial energy level to

a lower energy level. The wavelength of the emitted photon is

$$\lambda = \frac{c}{\nu} \qquad (2.12)$$

where c is the speed of light and ν is the frequency of the emitted photon, which is directly related to the change in energy of the electron, as such:

$$\nu = \frac{E_i - E_f}{h} \qquad (2.13)$$

Here, E_i and E_f are, respectively, the initial and final energy levels of the electron, and h is Planck's constant. Furthermore, numerous models formulated to describe atomic structure have shown that the energy levels for electrons in an atom are quantized.

1. The Bohr Model for Hydrogen

The simplest model of atomic structure, the Bohr model, could only accurately describe the radiation of single electron atoms such as hydrogen or singly ionized helium. Nonetheless, the Bohr model accurately predicts the wavelengths of all five known series of the hydrogen spectrum, and works equally well on singly ionized helium. Although certain postulates upon which the Bohr model is based have since been disproven, the model serves as a suitable "jumping off point" for describing the hydrogen spectrum, which is of particular importance in this thesis.

Bohr showed that the total energy of an electron "orbiting" the nucleus of an atom of atomic number Z could only take on discrete values

$$E_n = -\frac{mZ^2 e^4}{(4\pi\epsilon_0)^2 2\hbar^2}\frac{1}{n^2} \qquad n = 1,2,3,... \qquad (2.14)$$

Here, m is the electron mass, e is the electron charge, and $1/4\pi\epsilon_0$ is the Coulomb's Law

constant. $\hbar$ is Planck's constant over 2π. For hydrogen, $Z = 1$, and

$$E_n = -\frac{13.6}{n^2} \ eV \qquad n = 1,2,3,... \tag{2.15}$$

The integer n is the *quantum number*, and denotes the discrete energy level of the electron. $n = 1$, the lowest possible energy level, is considered the *ground* state, while higher energy levels are considered *excited* states.

2. Quantum Numbers

The definitions and descriptions put forth here are by no means complete. An in depth treatment of quantum numbers and degeneracy can be found in Eisberg and Resnick (1985).

The time-independent Schrodinger equation relates the quantum state of an electron to its total energy:

$$-\frac{h^2}{2\mu}\nabla^2\psi(r,\theta,\phi) + V(r)\psi(r,\theta,\phi) = E\psi(r,\theta,\phi) \tag{2.16}$$

Here, μ represents the reduced mass of the system, h is Planck's constant, and $V(r)$ is the Coulomb potential of the hydrogen nucleus. E is the total energy of the electron, as determined by Bohr for the quantum state n, and is called the *eigenvalue*.

The terms

$$-\frac{h^2}{2\mu}\nabla^2 + V(r) \tag{2.17}$$

comprise an operator known as the *Hamiltonian*, which is designated H, such that

$$H\psi(r,\theta,\phi) = E\psi(r,\theta,\phi) \tag{2.18}$$

$\psi(r,\theta,\phi)$ is the solution of the equation, called the *eigenfunction*. It is the product of the functions of the three independent variables r, θ, and ϕ, which describe the

11

position of the electron with respect to the nucleus in a spherical coordinate system:

$$\psi_{nlm_l}(r,\theta,\phi) = R_{nl}(r)\Theta_{lm_l}(\theta)\Phi_{m_l}(\phi)$$

(2.19)

As is evident from (2.19), the eigenfunctions are characterized by no less than three quantum numbers, designated n, l, and m_l. Possible values for the three quantum numbers are as follows:

$$
\begin{aligned}
n &= 1,2,3,... \\
l &= 0,1,2,...,n-1 \\
m_l &= -l,-l+1,...,0,...+l-1,+l
\end{aligned}
$$

(2.20)

The first quantum number, n, is the quantum number from the Bohr model, and describes the total energy of the electron. E_n is called the *eigenvalue*, and n is called the *principal* quantum number.

a.   *Orbital Angular Momentum*

Each electron orbit associated with a quantum number n has one or more associated values of angular momentum. The total angular momentum of the system, L, is quantized according to the quantum number l, termed the *azimuthal* quantum number, and is expressed as:

$$L = \sqrt{l(l+1)}\,\hbar$$

(2.21)

This only refers to the total angular momentum of an electron orbiting a nucleus. L_z, the z component of orbital angular momentum, is quantized according to m_l, and may assume the following values:

$$L_z = m_l\hbar$$

(2.22)

Orbital angular momentum of the electron is commonly represented in a vector model, which displays, for a single value of l, all possible states of orbital angular momentum as defined by m_l. Figure 2.3 below shows the vector model of orbital angular momentum for the state $l = 2$. Such vector models depict the possible angular momentum states as vectors of magnitude L, which may be located at any point about the z axis defined by a cone of height $\pm L_z$.
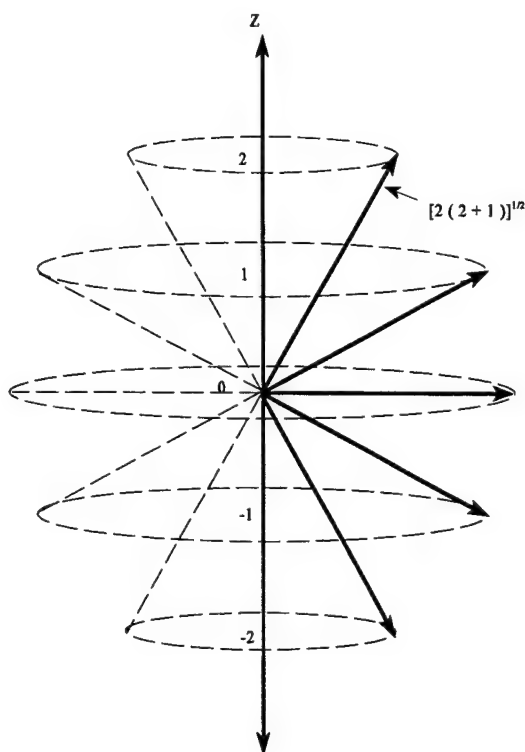
Figure 2.3. Vector Model of Orbital Angular Momentum for the State $l = 2$. Numbers are in units of $\hbar$. (From Eisberg and Resnick, 1985)

b. *Spin Angular Momentum*

In addition to orbital angular momentum, an electron posseses an intrinsic angular momentum, S, called its *spin*. Spin is quantized according to the quantum numbers s and ms, which may assume the follwoing values:

$$s = 1/2$$
$$m_s = \pm 1/2 \tag{2.23}$$

Spin angular momentum is quantized similar to orbital angular momentum, specifically:

$$S = \sqrt{s(s+1)}\,\hbar$$
$$S_z = m_s \hbar \tag{2.24}$$

c. *Total Angular Momentum*

The orbital and spin angular momenta of an electron are coupled through what is known as the *spin-orbit interaction*. This arises from an internal magnetic field created by the orbiting of the electron about the nucleus. This field is oriented in the same direction as $\mathbf{L}$, and interacts with the electron's spin magnetic dipole moment, which is oriented in the same direction as $\mathbf{S}$, and produces a torque. This torque serves to couple the orbital and spin angular momenta, causing them both to precess about their vector sum,

$$\mathbf{J} = \mathbf{L} + \mathbf{S} \tag{2.25}$$

Here, $\mathbf{J}$ is defined as the *total angular momentum* of the electron, and is quantized according to the quantum numbers j and m_j, according to the quantization rules

$$J = \sqrt{j(j+1)}\,\hbar$$
$$J_z = m_l \hbar \tag{2.26}$$

14

where

$$j = l + \frac{1}{2}, l - \frac{1}{2}$$
$$m_j = -j, -j+1, \ldots, +j-1, +j \qquad (2.27)$$

Total angular momentum of the electron can also be represented in a vector model, much like the one used to represent orbital angular momentum.

a. Degeneracy

From (2.20) it is readily apparent that for every value of n there are several different possible values of l and m_l. In a one electron atom, such as hydrogen, the form of the eigenfunction depends on the values of all three quantum numbers, but the energy eigenvalue depends only upon the value of the principal quantum number, n. Because of this, an atom can have states with completely different behavior as defined by the quantum numbers, but have the same total energy. This phenomenon is called *degeneracy*, and eigenfunctions corresponding to the same eigenvalue are called *degenerate*. For example, ψ_{200} and $\psi_{21\pm1}$ describe different states of a one electron atom, yet each state has the same total energy, $E_{n=2}$ as defined by the Bohr model. In reality, the spin-orbit interaction results in a minute difference in energy between states with the same l but different j quantum numbers. However, the difference is very small, on the order of 10^{-5} eV. (Eisberg and Resnick, 1985)

Table 2.1 below shows, for a one electron atom, all possible values of the quantum numbers for $n = 1, 2, 3$. From Table 2.1, it can be seen that for every value of l there are $(2l + 1)$ degeneracies, and for every value of n there are n^2 degeneracies.

15

n	1	2		3		
l	0	0	1	0	1	2
m_l	0	0	-1,0,+1	0	-1,0,+1	-2,-1,0,+1,+2
Number of degenerate eigenfunctions for each l	1	1	3	1	3	5
Number of degenerate eigenfunctions for each n	1	4		9		

Table 2.1. Possible Values of l and m_l for n = 1,2,3 (After Eisberg and Resnick, 1985)

3.   Spectral Radiation

An atomic electron will always seek to occupy a state with the lowest possible energy, within the limitations of selection rules and the Pauli exclusion principle. For the hydrogen atom, this energy level is the ground state, defined by the eigenfunction ψ_{100}. An atom in an excited state will, over time, make a series of transitions to lower energy levels until the ground state is reached.

Each transition to a lower energy level is accompanied by the emission of a photon of energy $E_i - E_f$, and frequency

$$\nu = \frac{E_i - E_f}{h} \tag{2.28}$$

The wavelength associated with the emitted frequency is called a *spectral line* or *line*, and the collection of lines resulting from all possible transitions within an atom is called the *emission spectrum* of the atom.

a.   *Hydrogen Spectral Lines*

The emission spectrum for hydrogen can be easily and accurately determined using the Balmer formula, which expresses the reciprocal wavelength of each

line as a function of initial and final energy states:

$$\kappa = \frac{1}{\lambda} = R_\infty (1/n_f^2 - 1/n_i^2)$$ (2.29)

where R_∞ is the Rydberg constant and is defined as:

$$R_\infty = \frac{me^4}{(4\pi\epsilon_0)^2 4\pi\hbar^3 c} = \frac{13.6\,eV}{2\pi\hbar c} = 1.097\times10^7\,m^{-1}$$ (2.30)

b.   The Balmer Series

The Balmer series is the family of lines arising from transitions to $n_f = 2$ from higher states ($n = 3,4,5,...,n = \infty$). The Balmer series has an infinite number of lines, ranging in wavelength from 6562.8 Å in the visible to the series limit ($n = \infty$) 3645.6Å in the near ultraviolet. 1Å = 1 angstrom = 10^{-10} meters. Table 2.2 shows some of the more prominent lines of the Balmer series. The Balmer series is one of five known series of hydrogen lines, each characterized by transitions to a particular n_f. The other four series are the Lyman ($n_f = 1$), Paschen ($n_f = 3$), Brackett ($n_f = 4$) and Pfund ($n_f = 5$) series.

Line Designation	n_i	λ (Å)
H_α	3	6562.8
H_β	4	4861.3
H_γ	5	4340.5
H_δ	6	4101.7
H_ϵ	7	3970.1
H_ζ	8	3889.1
H_∞	∞ (Series Limit)	3645.6

Table 2.2. The Balmer Series

The Balmer series is of particular importance here because of its widespread application in the study of Stark broadening. Particular attention will be paid

to the second line in the series, the H$_\beta$ line at 4861.33 Å, as it is the most widely studied wavelength in the theory of Stark broadening (Huddlestone and Leonard, 1965).

c. *Selection Rules*

Although the Balmer formula and the Bohr model accurately predict the lines of all five hydrogen series, they are nonetheless incomplete models. While they accurately predict the change in energy and wavelength of the resulting spectral line, they provide very little insight into the actual atomic transition that is taking place. Modern quantum theory has shown that a transition can only take place if it satisfies the following *selection rules*:

$$\Delta l = \pm 1$$
$$\Delta j = 0, \pm 1 \qquad\qquad (2.31)$$

In order for a transition to be possible between two energy levels n_i and n_f, their respective l quantum numbers may only differ by one, and their j quantum numbers can only differ by zero or one. Since the l degeneracy of the hydrogen atom causes total energy to be only dependent upon the principal quantum number n, the Bohr model need only address changes in the principal quantum number to successfully predict the spectrum of a one-electron atom.

However, if the l degeneracy is removed, as it is in the presence of an external electric field, the total energy of a quantum state becomes dependent upon l, and the Bohr model and Balmer formula can no longer accurately predict the resulting spectral lines. The removal of the l degeneracy due to an applied electric field is the mechanism that causes the Stark effect, after which the phenomenon of Stark broadening takes its name.

Figures 2.4 and 2.5 show two different representations of energy level diagrams for hydrogen, and the transitions that can result due to the applicable theories. Figure 2.4 shows the energy levels and transitions that are predicted by the Bohr model, as well as the locations of the corresponding spectral lines. Note the nonlinearity of the wavelength and frequency scale. Transitions that are predicted by the Bohr model but do

not occur are denoted by dashed lines. Figure 5 shows some of the allowed transitions in the Balmer ($n_f = 2$) series, taking into account selection rules.
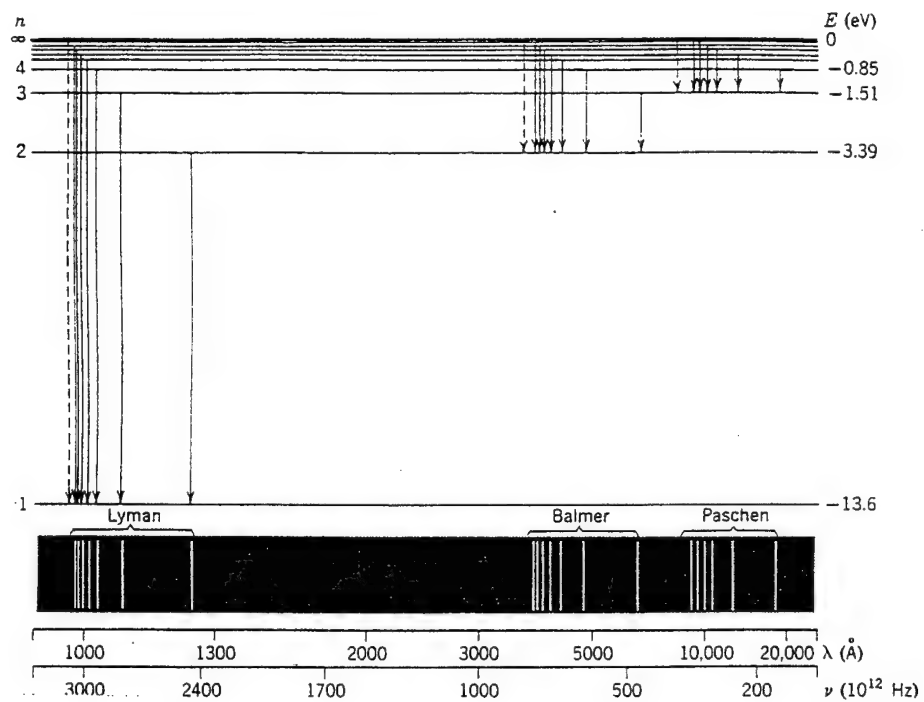
Figure 2.4. Energy Level and Transition Diagram for Hydrogen According to the Bohr Model. (Eisberg and Resnick, 1985)
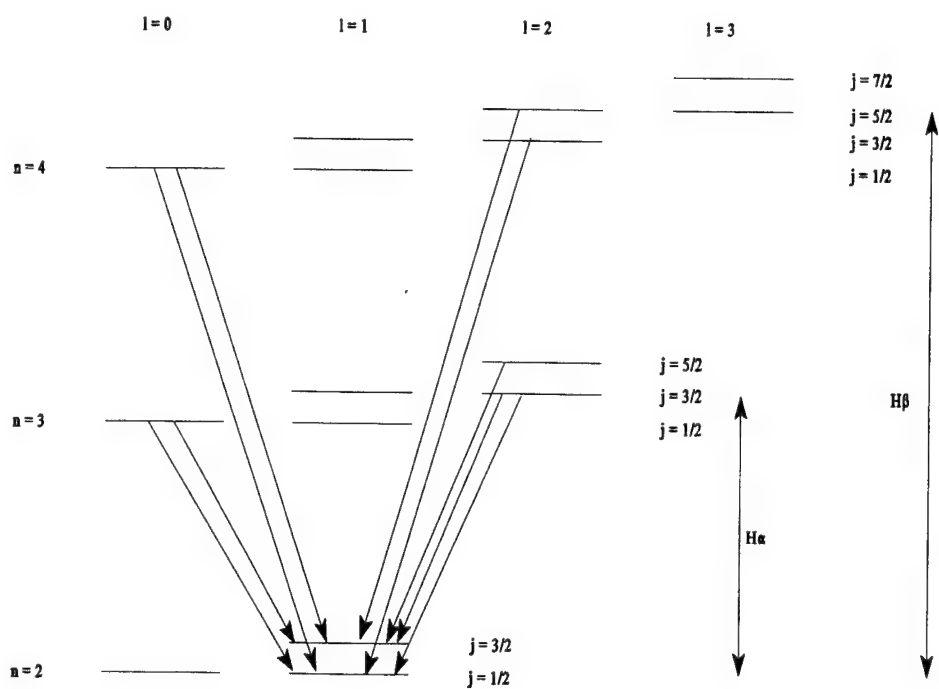
Figure 2.5. Some Allowed Transitions for the Balmer Series.

III. LINE BROADENING IN PLASMAS

The two major classes of line broadening are Doppler broadening, and collision broadening. While Doppler broadening relates to the velocity, and ultimately, the temperature of the radiating atom, collision broadening is the result of collisions on the atomic level with other particles, either charged or neutral. The two dominant causes of line broadening in plasmas are Stark broadening, due to the perturbation of the energy states of the emitting atom by the electric fields of nearby charged particles, and Doppler broadening, caused by the thermal motion of the emitter.

A. TERMS AND CONVENTIONS

1. Line Shape

Ideally, a spectral line is represented as a line of zero width at the wavelength at which it is emitted. However, even when completely isolated from its neighbors and shielded from all external fields, a transitioning atom will emit a line of finite width (Marr, 1968). The natural width of these lines tends to be on the order of hundredths or thousandths of an angstrom, although this is rarely the observed case. Typically, a line is broadened by one or more mechanisms, and takes on one of several distinct shapes known as a line shape.

Line shape, or line profile, is a term used to describe the distribution of intensity of a spectral line over wavelength or frequency. The shape is denoted $I(\Delta\lambda)$ or $I(\Delta\nu)$, where I is the intensity distribution.

$$
\begin{aligned}
\Delta\lambda &= \lambda - \lambda_0 \\
\Delta\nu &= \nu - \nu_0
\end{aligned}
\qquad (3.1)
$$

λ_0 and ν_0 are the wavelength and frequency of the emission, also called the *center* wavelength and frequency. $I(\Delta\lambda)$ can take on one of three different shapes.

21

a.   *Lorentzian Profile*

Also known as a "dispersion-type" (Huddlestone and Leonard, 1965) shape, the Lorentzian shape is the natural line shape of an unbroadened spectral line (Marr, 1968), and is represented by the function

$$I(\Delta\lambda) \propto \frac{1}{1 + \dfrac{\Delta\lambda^2}{\Delta\lambda_{1/2}^2}} \qquad (3.2)$$

$\Delta\lambda_{1/2}$, the *half width* of the profile, is the wavelength difference at which the intensity drops by a factor of two. $2\Delta\lambda_{1/2}$ is known as the full half-width of the profile. Lorentzian profiles are associated with collision broadened lines, of which Stark broadening is a type. A lorentzian profile is shown below in Figure 3.1.
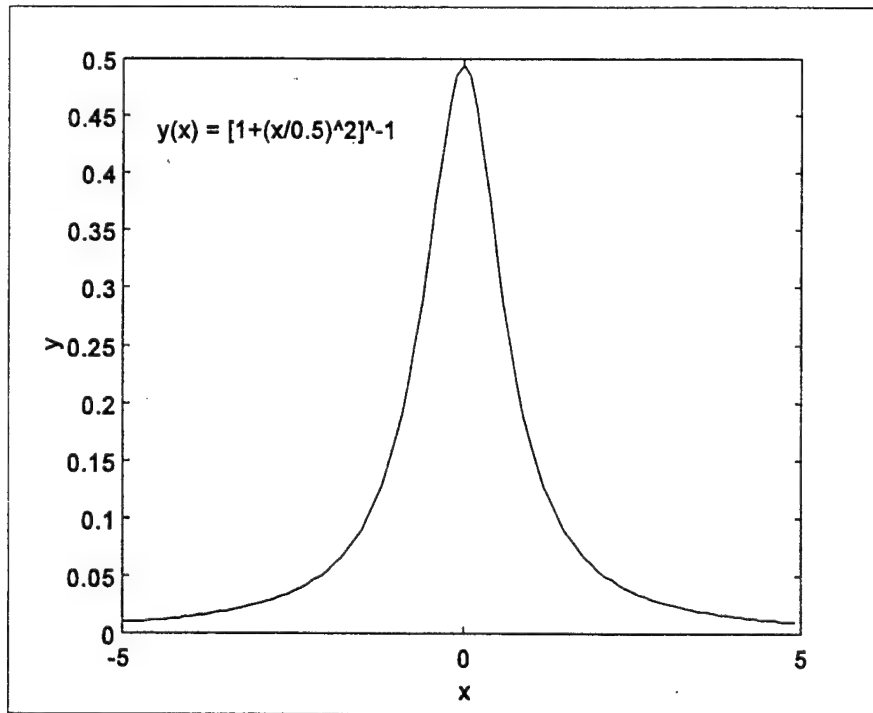
Figure 3.1. Lorentzian Profile, $\Delta x_{1/2} = 0.707$.

22

b.   *Gaussian Profile*

A Gaussian shape, also known as a Maxwellian distribution, takes the
form

$$I(\Delta\lambda) = I_0 e^{-\left(\frac{\Delta\lambda}{\Delta\lambda_D}\right)^2}$$

(3.3)

where I_0 is the intensity at the line center, and λ_D, the Doppler width, is the wavelength
difference at which the intensity is reduced by a factor of $1/e$. The half width of a
Gaussian line shape is

(3.4)

$$\Delta\lambda_{1/2} = \Delta\lambda_D\sqrt{\ln 2}$$

The term *Doppler width* is used here in reference to Doppler broadening, which produces
line shapes that are distinctly Gaussian (Griem, 1964). Doppler broadening will be
discussed in detail later in this chapter. An example of a Gaussian profile is shown in
Figure 3.2.
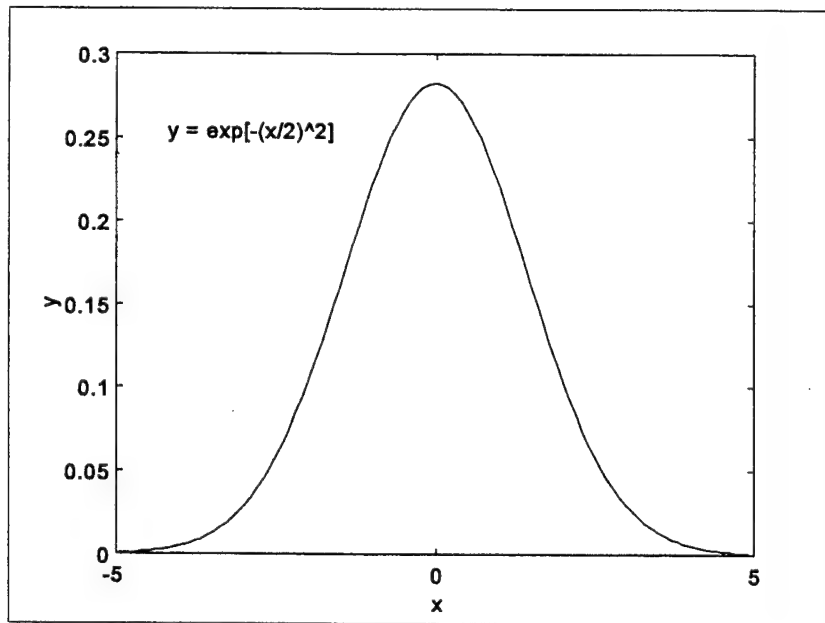
Figure 3.2. Gaussian Profile

c.   *Voigt Profiles*

In many instances, a spectral line will exhibit neither a purely Lorentzian nor a purely Gaussian shape, but will instead show features of both distributions. Such a profile is called a Voigt profile, and is formed by the convolution of a Gaussian with a Lorentzian profile:

$$I(\Delta\lambda) = \int_{-\infty}^{+\infty} I_D(\Delta\lambda) I_L(\Delta\lambda^* - \Delta\lambda) d(\Delta\lambda) \tag{3.5}$$

The resulting profile is expressed as a function of the dimensionless variable w (Marr, 1968):

$$I(\Delta\lambda) \propto \int_{-\infty}^{+\infty} \frac{e^{-y^2}}{a^2 + (w - v)^2} dy \tag{3.6}$$

where

$$w = \frac{\lambda - \lambda_0}{\Delta\lambda_D} \tag{3.7}$$

and a is called the *damping ratio* and is defined as the ratio of the Lorentzian to the Doppler half widths:

$$a = \frac{\Delta\lambda_L}{\Delta\lambda_D \sqrt{\ln 2}} \tag{3.8}$$

A Voigt profile will be the resultant line shape when both collision-type and Doppler broadening are present in a line profile. Examples of Voigt profiles with varying parameters can be seen in Figure 3.3.
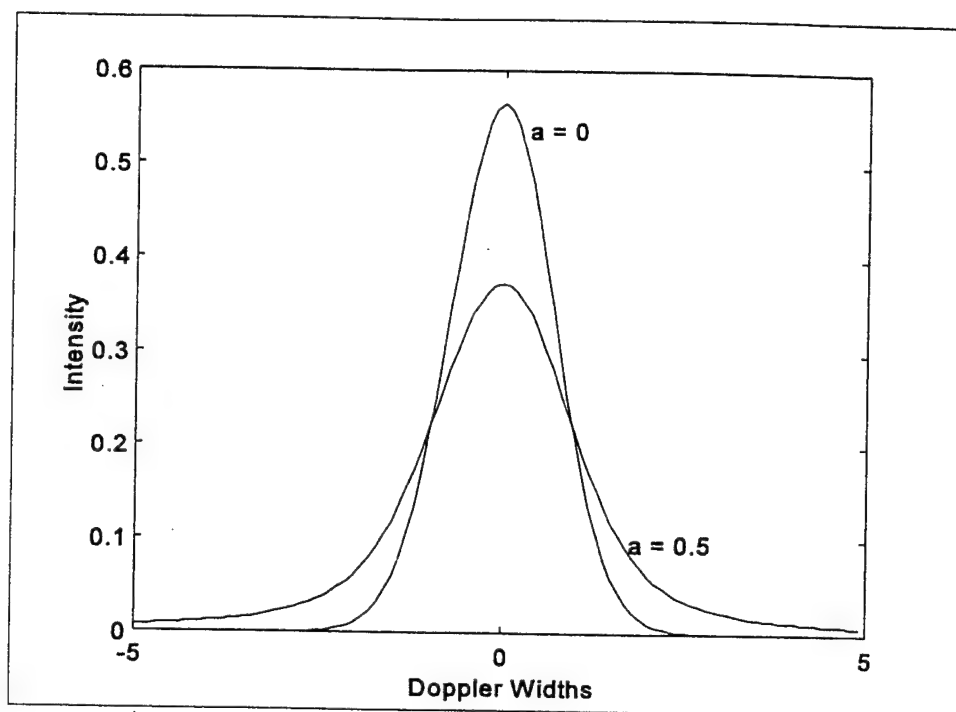
Figure 3.3. Voigt Profiles for Damping Parameter (a) of 0, 0.5

B.   DOPPLER BROADENING

Doppler broadening takes its name from the so-called Doppler effect, which states that radiation emitted from a source moving towards or away from an observer is shifted in frequency by

$$\Delta v \; = \; \pm v_0 \frac{v_s}{c} \qquad\qquad (3.9)$$

where v_0 is the frequency of the source at rest, v_s is the velocity of the source, and c is the speed of light. Radiation from a source moving toward an observer experiences a positive shift, while a negative shift occurs when the source is moving away from the observer. The resulting wavelength shift is also expressed as

$$\Delta \lambda \; = \; \mp \lambda_0 \frac{v_s}{c} \qquad\qquad (3.10)$$

25

where λ_0 is the unshifted wavelength. In a plasma, the random motions of radiating particles causes a Doppler shift in the emitted radiation, which manifests itself in a phenomenon known as Doppler broadening. Assuming the motion of particles within the plasma is of a thermal nature, the velocity distribution of the emitting atoms is Gaussian, and

$$\frac{dN}{N} = \frac{1}{\sqrt{\pi}} e^{-\left(\frac{v_s}{v}\right)^2} \frac{dv_s}{v} \tag{3.11}$$

represents the fraction of particles moving in the line of sight with velocities between v_s and $v_s + dv_s$, and $v = (2kT/m)^{1/2}$ being the most probable velocity. By substituting $\Delta\lambda$ for v_s from (3.10), and defining

$$\Delta\lambda_D = \frac{v}{c}\lambda_0 \tag{3.12}$$

(3.11) may be rewritten as:

$$\frac{dN}{N} = \frac{1}{\lambda_D\sqrt{\pi}} e^{-\left(\frac{\Delta\lambda}{\Delta\lambda_D}\right)^2} d(\Delta\lambda) \tag{3.13}$$

Lastly, assuming the total intensity, I_t is proportional to N, and $I(\Delta\lambda)d(\Delta\lambda)$ is proportional to dN, the formula

$$I(\Delta\lambda) = \frac{I_t}{\lambda_D\sqrt{\pi}} e^{-\left(\frac{\Delta\lambda}{\Delta\lambda_D}\right)^2} \tag{3.14}$$

is arrived at for the line shape of a Doppler broadened line.

It is apparent from

$$\Delta\lambda_D = \frac{\lambda_0}{c}\sqrt{\frac{2kT}{m}} \qquad\qquad (3.15)$$

that if the Doppler width of a profile is known, the plasma temperature, at least for the emitting atoms, can be determined. Doppler broadening can also result from the bulk motion of the plasma, and is evident in many pulsed plasmas (Huddlestone and Leonard, 1965).

C.   STARK BROADENING

Unlike Doppler broadening, Stark broadening is only a single category of what is known as *collision or pressure broadening*. Collision broadening is largely due to the interaction of the emitter with surrounding particles, and is subdivided into three distinct types:

1. *Resonance broadening* due to interaction with atoms of the same kind.

2. *Van der Waals broadening* due to interaction with neutral molecules or atoms of different species.

3. *Stark broadening* due to interaction with charged particles (ions and electrons).

Named after the so-called Stark effect, Stark broadening is the broadening of the natural (Lorentzian) shape of a spectral line due to the interaction of the emitter with the Coulomb forces of nearby ions and electrons, which are present in abundance in dense plasmas.

1.   Stark Effect

The Stark effect takes its name from the investigations of Stark in 1913 on the emission spectrum of hydrogen in the presence of an electric field (Marr, 1968). Stark discovered that a splitting of spectral lines occurs when the radiators are in the presence of an electric field, due to the removal of degeneracies in the unperturbed eigenvalues of an atomic electron. The quantum mechanical treatment of the Stark effect is rather complex compared to other splitting mechanisms such as the Zeeman effect, and is not

needed in the analysis of a spectrum (Herzberg, 1944). The theory will therefore be presented in its elementary form, with the appropriate references made to quantum mechanical conventions.

a.   *Elementary Stark Effect Theory*

In the presence of an electric field of strength F, the magnetic moment associated with the total angular momentum, **J**, of an atom is unaffected. However, the field will polarize the atom, by displacing the positively charged nucleus from the center of gravity of the negative charge distribution. This results in the creation of an electric dipole moment proportional to F, say αF, where α depends upon the orientation of the electron charge distribution to the field, and is therefore a function of **J**. This is shown in Figure 3.4 where the nucleus N is shown separated from the center of negative charge S (Marr, 1968).

A precession of **J** about the electric field direction occurs due to the interaction of the electric dipole with the electric field, such that the component M_J in the direction of the field remains constant. The rate of precession increases with increasing F, and the energy change for given angular momentum state **J** is given by the product of the field strength and the electric dipole,

$$\Delta E = K M_J F^2 \tag{3.16}$$

where K is a constant denoting a fractional portion of M_J (Herzberg, 1944).

It can be seen from (3.16) that the energy shift due to the Stark effect is proportional to the square of the field strength. This is termed the *quadratic* Stark effect. Also, it is of note that term components that differ in the sign of M_J have the same energy, as reversing the rotation of an orbiting electron (changing M_J to $-M_J$) does not alter the electric dipole moment.
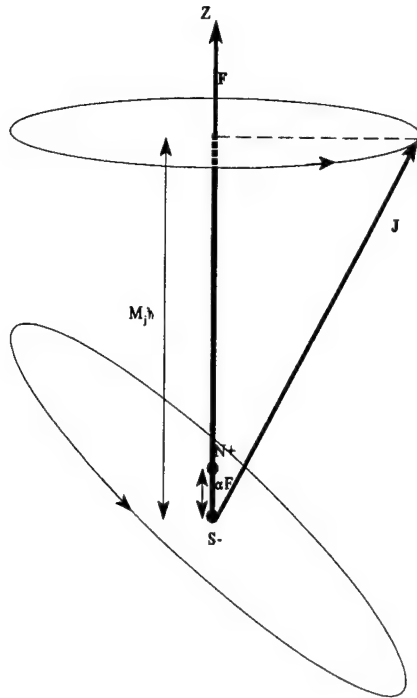
Figure 3.4. Vector Diagram for Electric Field F Coupling for Atoms. S is the center of gravity of the electrons with resultant angular momentum J perpendicular to the orbital plane. (After Marr, 1968)

b.   *Stark Effect for Hydrogen*

Unlike other atoms, hydrogen exhibits a strong *linear* Stark effect, that is, the energy shift increases linearly with field strength. If a perturbing electric field of strength F is applied to an atom, the potential of that field is:

$$eF_z = eFr\cos\theta \qquad (3.17)$$

Time independent perturbation theory states that the total energy of a state n under the influence of a perturbing potential is

$$W_n = E_n + H'_{n,n} + \sum_n \frac{|H'_{n,n'}|^2}{(E_{n'} - E_n)^2} + \ldots \qquad (3.18)$$

29

where $H'_{n,n'}$ is the interaction Hamiltonian between energy states n and n', defined as

$$H'_{n,n'} = \int \psi_{n'} v \psi_n d\psi \qquad \cdot \qquad (3.19)$$

(3.19) defines the interaction between the two states n and n' due to a perturbing potential, v. In most atoms subject to electric fields, the first order term ($H'_{n,n}$) of the perturbation vanishes, and the quadratic term must be used to a first approximation. However, if states are degenerate to the extent that two states with different l quantum numbers have the same energy (as in the hydrogen atom) it is possible to have a nonzero first order effect provided that $\Delta l = \pm 1$ and $\Delta m \neq 0$ (Marr, 1968).

Both the Bohr theory and modern quantum mechanics show that, for hydrogen, an energy level n splits into $2n - 1$ equidistant energy levels, the energy difference of which increase linearly with field strength (Herzberg, 1944).

2.   Stark Broadening Theory

In the presence of a significant quantity of ions and electrons, as in a plasma, a radiator is subjected to electric fields which consequently perturb its normal energy levels by way of the Stark effect. Varying electric field strengths within the plasma cause a spreading of the Stark levels in individual atoms, resulting in a statistical broadening of the spectral lines, known as Stark broadening. In dense plasmas, Stark broadening is the predominant form of line broadening.

If the perturbing ion or electron is treated as a classical particle, then the duration of each perturbation in a statistical distribution of perturbing particles is defined by

$$\tau_s = \rho/v_{av} \qquad (3.20)$$

where ρ is the impact parameter of the perturbing particle, and v_{av} is the average velocity of the perturber. Due to the large difference in the velocities of the fast moving electrons and slow ions, τ_s varies greatly for the particles. This resulted, initially, in two theories of Stark Broadening, called the *impact approximation* and the *quasi-static approximation*.

a. Quasi-Static Approximation

The quasi-static approximation is used in calculating the Stark broadening due to ions, as τ_s is generally larger than the average time between collisions with ions. For that reason, the motion of ions may be neglected completely, and a static Stark effect is assumed, taking into account the statistical distribution of electric fields at the radiating atom (Marr, 1968).

In computing a line profile using the quasi-static approximation, the splitting of the line resulting from the Stark effect is first calculated, which is defined as:

$$\Delta \nu_{if} = C_{if} F^{\mu} \tag{3.21}$$

where $\mu = 1$ for the linear Stark effect, 2 for quadratic, and C_{if} is the Stark coefficient for transitions between initial state i and final state f in a radiating atom, and is derived from applying perturbation theory (Griem, 1964). The line splitting is then averaged over the probability distribution of all different electric microfields within the plasma, denoted

$$W_H(F) = \frac{1}{F_0} W_H\left(\frac{F}{F_0}\right) = \frac{1}{F_0} W_H(\beta) \tag{3.22}$$

F_0, called the normal or Holtsmark field strength (Griem, 1964), depends only upon ion density and is defined as

$$F_0 = \frac{2.61e}{4\pi\epsilon_0} N^{2/3} \approx 1.25 \times 10^{-9} N^{2/3} \quad V/cm \tag{3.23}$$

N is the ion density of the plasma.

b. Impact Approximation

The impact approximation for Stark broadening must take into account the infrequent and short-lived interactions of the radiator with highly mobile electrons, and therefore cannot assume a time-independent perturbation as in the quasi-static

31

approximation. Determining an impact-broadened line profile first requires the solution of a time-dependent Schrodinger equation of the form

$$i\hbar \frac{d\chi(t)}{dt} = [H_A + V_e(t)]\chi(t) \qquad (3.24)$$

where H_A is the Hamiltonian of the unperturbed radiator, and $V_e(t)$ is the potential of the perturbing electron. $\chi(t)$ describes the state of the emitting electron, and is defined as

$$\chi(t) = T_A(t,0)\chi(0) \qquad (3.25)$$

where $T_A(t,0)$ is called the time evolution operator, which relates wave functions at time t to those at $t = 0$ (Griem, 1964).

This equation must be solved for T_A for all $V_e(t)$ produced by perturbers passing with various velocities, impact parameters, and times of closest approach. These solutions are then substituted into a correlation function which is statistically averaged over all possible perturber trajectories. Finally, the Fourier transform of the correlation function is taken in order to obtain the impact broadened line profile. (Griem, 1964)

3. Stark Profiles

In order to generate a Stark broadened line profile using both the impact and quasi-static approximations, the quasi-static theory is first applied, subjecting the radiating atom to a static field causing energy level shifts and line splitting. After that, the electron broadening is superimposed upon the resulting Stark patterns (Huddlestone and Leonard, 1965). Stark profiles have been generated and tabulated, most notably for the Balmer series of hydrogen, for use in plasma spectroscopy. Stark broadening produces a Lorentzian line profile.

32

The tabulated profiles themselves are one half of a symmetrical profile, and are generally presented as functions of $S(\alpha)$ versus α. α is known as the *reduced wavelength*, and is expressed as

$$\alpha = \frac{\Delta\lambda}{F_0} \approx -\frac{\Delta\omega\lambda_0^2}{2\pi c F_0} \qquad (3.26)$$

F_0 is the Holtsmark field strength, dependent upon ion density. From $S(\alpha)$, a profile in the wavelength scale can be obtained from

$$I(\lambda) = S(\alpha)\frac{d\alpha}{d\lambda} = F_0^{-1} S(\alpha) \qquad (3.27)$$

Stark profiles for hydrogen have been extensively calculated using numerous approximations. The most accurate Stark tables for hydrogen have been generated using the "Unified Classical Path Theory", often called the "Unified Theory" of Stark broadening, developed by Vidal, Cooper, and Smith (1970). While adhering to the quasi-static approximation for ions, the Unified Theory of Stark broadening develops a more complex model for electron collisions. This gives better agreement with experimental data than the impact theory does, particularly in the line wings and transition region between the line wings and line center. Stark profiles for a given spectral line are normally presented in tabular format according to electron density and temperature of the plasma environment of the radiator. The profiles are well known for several lines of the Balmer series, and have been computed for other hydrogen series as well, most notably the Lyman series. All computed profiles are normalized such that

$$\int_{-\infty}^{+\infty} S(\alpha)\,d\alpha = 1 \qquad (3.28)$$

33

The most notable and distinguishing aspect of Stark broadened line shapes occurs at relatively high electron (ion) densities ($N_e \geq 3 \times 10^{14}$ cm^{-3}) where the Stark effect due to ions is great enough that the spectral line splits. When this happens, the line appears as two Lorentzian lines side by side, which overlap at the line center. Figure 3.5 shows the comparison of theoretical and experimental Stark profiles for the H$_\beta$ line at an electron density of 6.4×10^{16} cm^{-3}. Generally, the splitting of the line is stronger in theory than in experiment (Vidal, Cooper and Smith, 1972), although in Figure 3.5 it is quite evident in both the measured and theoretical profiles.
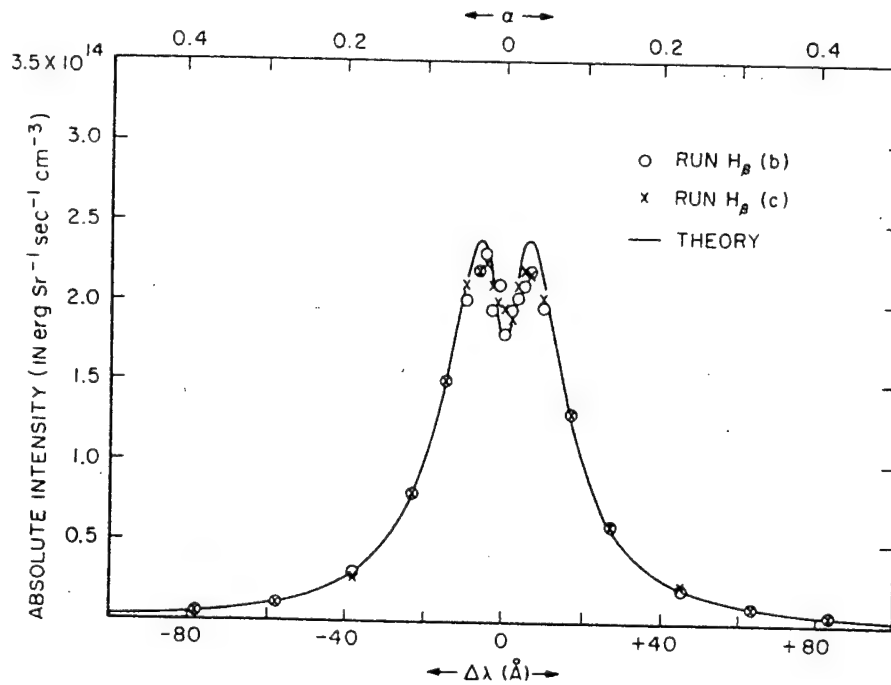
Figure 3.5. Comparison of Experimental and Theoretical Stark Profiles of the H$_\beta$ Line. $N_e = 6.4 \times 10^{16}$ cm^{-3}, $T_e = 12,210$ K. (From Huddlestone and Leonard, 1965)

4. Electron Densities

The most common use of Stark broadening as a diagnostic tool is in determining electron densities in plasmas (Huddlestone and Leonard, 1965). The most common way

of doing this is by comparing the full half width of a spectral line with the half widths of computed Stark profiles. Electron density is then determined using the relation

$$\Delta\lambda_{1/2} = 2F_0\alpha_{1/2} = 2.5\times10^{-9}\alpha_{1/2}N_e^{2/3} \quad \text{Å} \tag{3.29}$$

where $\Delta\lambda_{1/2}$ is the full half width of the line profile, and $\alpha_{1/2}$ is the value of α at which $S(\alpha)$ is one half its maximum value. $\alpha_{1/2}$ must be retrieved from the theoretical profile. This has already been done for various hydrogen lines, at various electron densities and temperatures, by Griem (1974). N_e is the electron density of the plasma. Using half width comparison, errors on the order of 10 - 15% can be expected, the lower limit being achievable for lower (10^{15} cm^{-3}) electron densities (Griem, 1964).

The second way of determining electron densities is by a least squares fit of an observed line profile to the theoretical Stark profiles. This method is the better of the two for higher electron densities ($\sim 10^{16}$ cm^{-3}) where splitting of spectral lines (especially the H$_\beta$ line) becomes significant. At lower electron densities (10^{15} cm^{-3}), error should be on the order of 5%, while an upper limit of 10% error can be expected for higher electron densities (Vidal, Cooper and Smith, 1972).

D.   ELECTRON DENSITY DETERMINATION IN PLASMAS

Very rarely will a spectral line emitted in a plasma be either purely Doppler- or Stark broadened. In fact, this is almost never the case; both forms of line broadening will invariably contribute to the line shape, and a Voigt profile will be the result. Before Stark broadening analysis can be applied to the spectral line, the Voigt profile must be analyzed to determine the extent to which each broadening mechanism is present, and the Doppler broadening must be factored out of the line profile.

1.   Half Width Estimation

When concerned only with the half-width of the observed line profile, it is sufficient to determine the Voigt parameters which best fit the observed profile, from which the Lorentzian and Gaussian half-widths can be extracted, and density and

35

temperature can be determined. The relationships between the Stark, Doppler, and observed half-widths of line profiles are presented in Appendix C.

Once the Stark half width of the profile is known, it can be compared to the known half widths of theoretical Stark profiles, which are tabulated as functions of N_e and T in Appendix III of Griem (1974) for several hydrogen and ionized helium lines. Given a reasonable value of T, either measured or determined from the Doppler width of the profile, and the Stark width of the observed profile, an electron density can be interpolated from the half width tables presented in Griem (1974). Figure 3.6 shows, for H_β, electron density versus half width for $T = 5000$ and 40000 K .
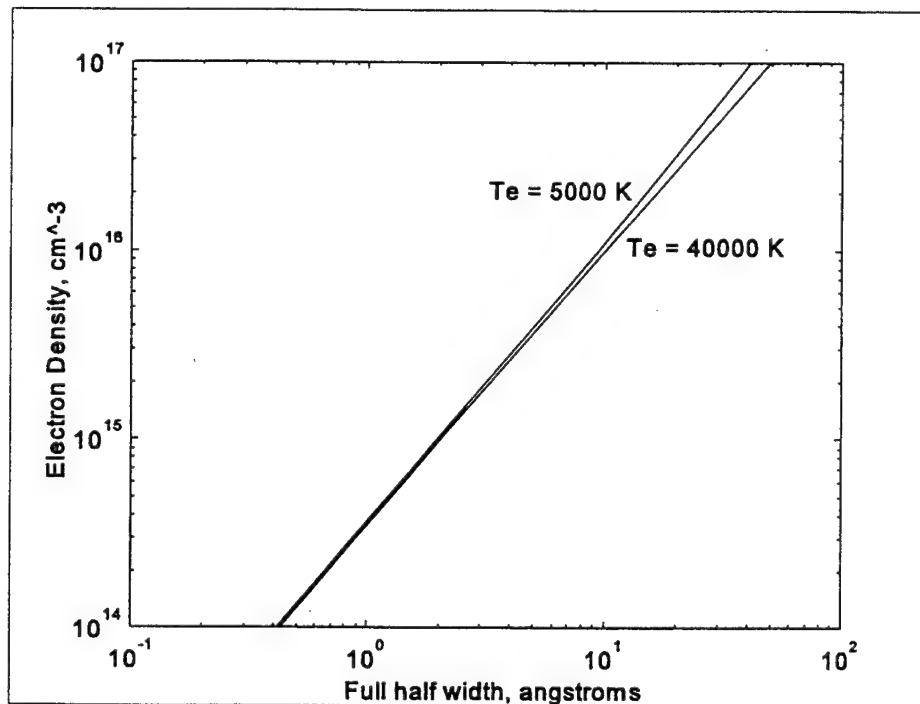
Figure 3.6. Electron Density Versus Full Half Width of the H_β Line for $T = 5000$ and 40000 K.

IV. EXPERIMENT SETUP

A.   CATHODE TEST FACILITY

The cathode test facility (CTF) at NASA-JPL is designed to observe and analyze cathodes under the simulated operating conditions of an MPD thruster. It contains all the necessary hardware and software to observe and record line profiles emitted from the plasmas generated in the facility. A complete description of the CTF is presented in Goodfellow (1996).

1.   Vacuum Chamber

The main component of the cathode test facility at NASA-JPL is a stainless steel vacuum chamber, 0.5 m in diameter and 2.4 m long, consisting of four water-cooled, cylindrical segments. A water-cooled, copper liner is inserted in the middle two segments to facilitate long duration cathode operation.

The cathode fixture is mounted on the vacuum chamber door, and consists of two coaxial tubes, electrically isolated from each other and the door. The cathode itself is clamped to the inner tube, which serves as the current feed for cathode operation. The cathode protrudes through a water cooled copper disk mounted on the end of the outer tube. The propellant gas is injected between the two tubes, and enters the discharge chamber (the first segment of the vacuum chamber) through an annulus formed around the base of the cathode. The cathode itself is 76 mm in length and 9.5 mm in diameter with a hemispherical tip, and is made of 2 percent thoriated tungsten.

The anode is a water cooled copper ring 7.6 cm in diameter, which is mounted on a flange between the first two segments of the vacuum chamber, from which it is electrically isolated. The last segment of the vacuum chamber contains a heat exchanger composed of water-cooled, finned copper tubing, which cools the exhaust before it enters the pumping system. Several optical ports line both sides of the chamber, providing access to the discharge chamber (particularly the cathode region itself) and the plasma plume. The rear of the chamber has a port which allows viewing of the cathode tip and plume along the axis of the tank.

37

The chamber is pumped down using a 610 liter/sec Roots blower, backed by a 140 liter/sec Stokes mechanical pump. Vacuums of less than 0.13 Pa (0.975 mTorr) can be achieved without propellant flow into the chamber, while a vacuum of approximately 80 Pa (0.6 Torr) can be achieved with an argon flow rate of 0.75 g/s (Goodfellow, 1996). Typical operating pressures during the experiment ranged from 11 Torr (1.467 kPa) to 30 Torr (4 kPa). Pressure in the discharge chamber was controlled either by adjusting propellant gas flow rate into the chamber, or by adjusting a gate valve between the chamber and the pumps.

Power to the arc is supplied from two Miller welding power supplies, each capable of supplying a continuous 1500 A at 60 V, or 2000 A at 50 V for up to 20 minutes. The initial arc breakdown is achieved with a 4 A, 850 V start supply.

2.   Tank Instrumentation

Arc current is monitored with precision shunts replacing the factory shunts on the Miller power supplies. Terminal voltage is measured at the current feedthroughs into the vacuum tank.

A Sierra Instruments Side-Trak Model 830 flow meter and a Micromotion Model D6 flow meter are used to monitor propellant flow into the thrust chamber. Propellant flow is controlled with a throttling gate valve located upstream of the inlet to the cathode fixture. An MKS Baratron capacitance manometer (0 - 133 Pa range) is used to monitor tank pressure.

The above parameters, as well as various system temperatures (cathode, anode, etc.) were monitored and recorded with a Macintosh computer utilizing LabView software and Opto-22 data acquisition hardware.

3.   Data Collection Equipment

A system for performing emission spectroscopy within the plasma plume was already in place in the cathode test facility. A lens was mounted outside an optical port at the thrust chamber, which focussed an image of the cathode on a screen. The inlet to a length of 100 micron diameter fiber optic cable was located at the center of the screen, flush with the surface. The image screen and fiber inlet were both mounted on a

38

micrometer-operated translation stage, which allowed the fiber inlet to be placed at any point within the image. The translation stage allowed adjustments in position to less than 0.5 mm.

Figure 4.1 shows a basic schematic of the data collection system. Light exiting the fiber was focused on the entrance slit of a one meter McPherson scanning monochromator. A 1200 groove/mm grating was used in the monochromator to disperse the light, and the variable entrance and exit slits were typically set at 30 microns.
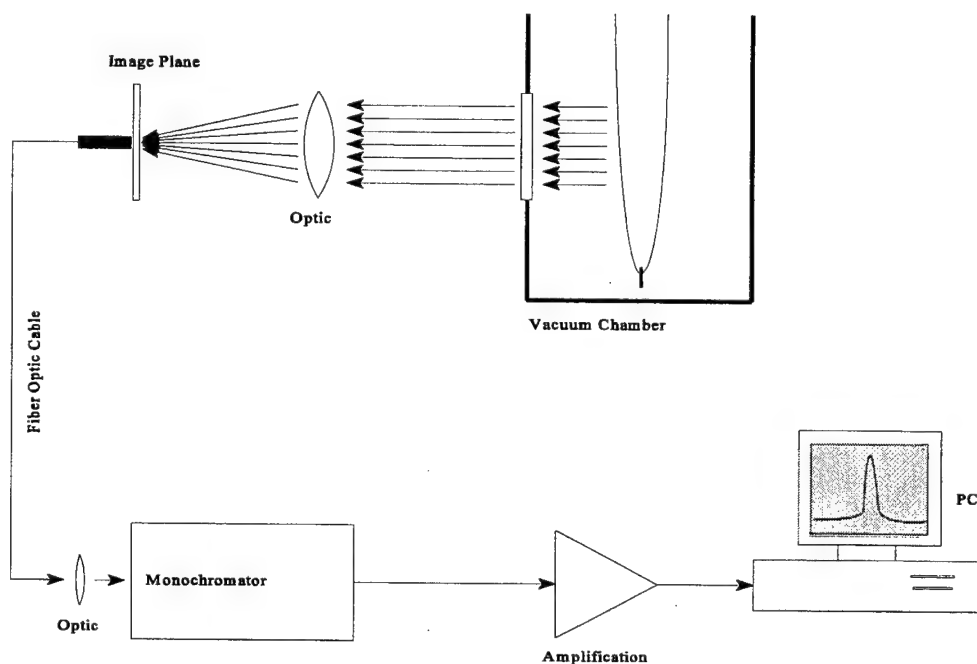
Figure 4.1. CTF Data Collection Equipment Setup.

Spectral resolution of the spectrometer is on the order of 1 Å. The output of the monochromator is amplified and stored as a voltage in a Macintosh computer, again using LabView software.

B. DATA COLLECTION

Data were gathered while the CTF was operating on an argon plasma, with small amounts of hydrogen (10 to 15% by volume) intermixed to allow observation of the H_β line. Under normal operating conditions, the plasma arc flows from the tip of the cathode, forming a cathode jet as defined in Chapter II. Sets of hydrogen line profiles for analysis were gathered from within this cathode jet. The scanned wavelength interval was from 4856Å to 4866Å, to allow inclusion of as much of the wings of the line as possible without serious overlap of nearby argon lines.

Initially, the horizontal micrometer translation stage was adjusted so that the inlet to the fiber optic cable was located directly off the tip of the cathode in the image plane. From this location on the cathode axis, the image plane could be translated vertically, so that the fiber inlet moved radially within the plasma plume. The vertical micrometer was adjusted in increments of 0.083 in (2.108 mm) between readings, which were taken in sets of 31. One reading was taken on the cathode axis, and 15 readings were taken to either side, up or down, of the cathode. Thus, a set of 31 readings covered a "sliver" of the plasma jet 2.49 in (63.246 mm) in diameter, centered about the cathode axis.

1. Data Format

As stated above, a 10 Å interval was scanned about the location of the H_β (4861.33 Å) line, from 4856 to 4866 Å at a resolution of 500 data points per angstrom. Each scan was stored on a Macintosh personal computer, using LabView software, as a file consisting of two arrays - wavelength, recorded in angstroms, and intensity, recorded as a voltage level. Each array consists of 5000 double precision floating point data values. For bookkeeping purposes, each set of scans was given a group name, and operating conditions such as argon/hydrogen flow rates, pressure, voltage and current were also recorded for each set of data. The cathode temperature profile was also monitored during data collection.
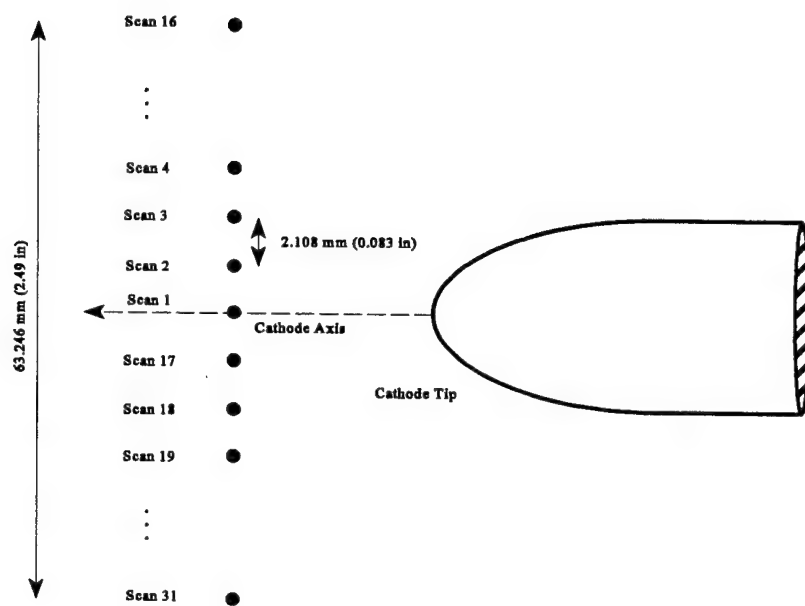
Figure 4.2. Scan Location With Respect to Cathode Tip.

V. ANALYSIS

In order to determine electron temperatures and denisities from the scanned line profiles, a computer program to determine characteristic line widths (both Doppler and Stark) was written in Interactive Data Language (IDL). Sequentially reading all 31 files in a data set, the program attempts to curve fit a Voigt profile to each line in order to estimate the parameters needed to extract the appropriate line widths. The appropriate characteristics are then determined either by a simple formula in the case of temperature, or by interpolation of tabulated theoretical data in the case of electron densities. Three separate sets of data were analyzed, varying in distance from the cathode tip and operating parameters, for which an overview of the analysis is given in this chapter. A documented listing of the IDL program is presented in Appendix A, and tabulated results of the analysis are presented in Appendix B.

A. ANALYSIS PROGRAM

The analysis program consists of eleven procedures which perform the tasks of reading and preparing the data, determining the contributions of Doppler and Stark effects to line width, calculating the electron temperatures and densities, and storing the results in a single data file for a set of scans. The majority of the procedures are used in the fitting of the data and determination of line widths. The program is initiated with a single call to a master procedure, called LINBROAD, which executes the above described functions in order. In turn, LINBROAD executes three sub-procedures:

1. FITFILE, which fits the appropriate Voigt profile to the scan and determines the Stark and Doppler widths of the line profile.

2. NETE, which takes the line widths output from FITFILE and computes the electron temperature and density of the profile.

3. STORIT, which writes the results to a data file with a user-specified name.

The first two procedures in turn call one or more sub-procedures of their own to accomplish their tasks.

43

1. FITFILE

FITFILE is an iterative procedure which first reads each data file one at a time using a procedure called GETFILE. Following the input of a single data file, FITFILE successively fits Voigt profiles to the data, adjusting the guessed Doppler width while keeping track of the Chi-Squared parameter of the fit, until a minimum Chi-Squared is reached, indicating a best fit.

Once a best-fit Voigt profile is found, the HALFWIDTH procedure is called in order to determine the half-width of the fit. Following that, the GETPAR procedure is executed to determine the fractional contribution of both Doppler and Stark broadening to the line width. The PROWIDTH procedure is then executed, which determines the full half width of the data. Lastly, FITFILE computes the Doppler and Stark widths of the data from the outputs of the GETPAR and PROWIDTH procedures.

a. GETFILE

GETFILE first reads the data file and chops off the first and last 200 data points in each array (wavelength and intensity), as the extreme wings of the scanned profile contain significant portions of neighboring argon lines which would otherwise adversely affect the fitting of the data. The procedure PROFCOR is called, which initially fits a Lorentzian profile to the data in order to determine the location of the line center. PROFCOR also determines an offset parameter, as the voltage (intensity) levels of the scan settle into negative values out in the line wings, which must be corrected for.

After the intial fit, the profile is further reduced in size to 3000 data points, and the profile spans 3Å to either side of the line center. The profile is then "folded" in half about the line center, averaged and then "unfolded" to produce a smoother, less "noisy" profile to accomodate the fitting of a Voigt profile.

b. GETPAR

Once a Voigt profile has been fitted to the data and the half width of the Voigt profile is determined, GETPAR is called to determine the relative contributions of Doppler and Stark broadening, based upon the Doppler width and half width of the fitted Voigt profile. This is done by executing a second-order polynomial fit of the ratio of the

44

Lorentzian half width to the full Voigt half width as a function of the ratio of Doppler half width to the full Voigt half width. The data to be fitted is presented in Huddlestone and Leonard (1965), and is reproduced in Appendix C.

c. PROWIDTH

PROWIDTH determines the full half width of the observed profile by first dividing the data into bins of 20 points each and taking the average of those bins, reducing the profile from 3000 to 150 points, and then finding the location of the bin on either side of the line center that most closely represents the half width. The right and left side half widths are then added to produce the full half width of the profile which, along with the ratios determined in GETPAR, is used to compute Doppler and Stark full half widths.

2. NETE

Given values for the Doppler and Stark widths of the line profile, NETE determines first the temperature, and then the electron density of the plasma. The temperature determination is easily accomplished by manipulating equations (3.4) and (3.15), giving

$$T_e = \frac{m}{2k\ln 2}\left(\frac{-c\Delta\lambda_D^{1/2}}{\lambda_0}\right)^2 \quad K \tag{5.1}$$

where $\Delta\lambda_D^{1/2}$ is the Doppler half width.

Electron densities are determined by interpolation of a table of theoretical Stark widths (in log space) as a function of temperature, as presented in Appendix III of Griem (1974). The portion of this table used is presented in Appendix C. The Stark widths for a given electron density as a function of electron temperature are fitted with a cubic spline, which is then interpolated for the temperature determined in (5.1). The spline is performed in log space with respect to temperature, resulting in the log of the electron density as a linear function of the log of the Stark width. A linear interpolation is then

performed for the log of the observed Stark width of the profile. The inverse logarithm of this interpolated value yields the electron density for the profile.

3. STORIT

After the electron densities and temperatures have been determined for a data set, STORIT writes the density and temperature vectors, as well as the full half width, Doppler and Stark widths, and the ratios of the Doppler and Stark widths to the full half width to a file with a user-specified name. STORIT also records the distance of each measurement from the cathode axis.

B. DATA REPRESENTATION

Each set of data is given a name for identification, consisting of the letters "CTF", for the cathode test facility at JPL, followed by a number which designates, in sequence, the running of the CTF for that purpose. For example, the data set CTF144 denotes the 144th running of the facility for gathering data. The three data sets analyzed here are CTF's 144, 145, and 146.

For each data set, operating conditions which may have some bearing on the analysis results are recorded. These are argon and hydrogen flow, in SLPM, tank pressure in Torr, and operating voltage and current.

Scans within a data set are numbered sequentially, from 1 to 31, with the file name "scan1", "scan2", etc., "scan1" being located on the cathode axis. Scans 2 through 16 make up the 15 scans above the cathode, and scans 17 through 31 lie below.

C. DATA ANALYSIS RESULTS

Of the three sets of data analyzed, one, CTF144, was taken at a location just off the tip of the cathode, while the remaining two were taken at a distance of approximately one half inch (1.27 cm) from the cathode tip. Tank pressure, hydrogen to total volume flow ratio, voltage and current were similar for CTF144 and CTF145, with CTF146 being taken at slightly higher values. While differing in numerical values, electron density and temperature behavior across the plasma plume were similar for all three data sets. Table 5.1 summarizes the operating conditions and extreme values for electron density and temperature for all three data sets.

46

Data Set	CTF144	CTF145	CTF146
Distance from Cathode	0 cm	1.27 cm (0.5 in)	1.27 cm (0.5 in)
Argon/Hydrogen Flow Rate	6.08 Ar 0.8 H_2	6.07 Ar 0.9 H_2	6.12 Ar 1.0 H_2
Pressure	12.25 Torr	11.8 Torr	21.4 Torr
Volatge	17.6 V	17.8 V	22.9 V
Current	1400 A	1400 A	1400 A
Max T Min T	8600 K 6200 K	7200 K 5000 K	15600 K 12900 K
Max N_e Min N_e	2.63×10^{14} cm^{-3} 2.30×10^{14} cm^{-3}	2.41×10^{14} cm^{-3} 2.14×10^{14} cm^{-3}	3.95×10^{14} cm^{-3} 3.61×10^{14} cm^{-3}

Table 5.1. Summary of Operating Conditions and Analysis.

Figures 5.1 and 5.2 below show the radial electron density and temperature profiles of all three data sets. All results were obtained using LINBROAD. Radius from the cathode axis is represented on a linear scale and electron density and temperature on a logarithmic scale. Apart from small fluctuations in N_e and T_e, all three data sets are reasonably well behaved. They suggest that the density and temperature distributions across the cathode jet were nearly constant. No apparatus presently exists at the NASA-JPL cathode test facility for direct measurement of electron densities and temperatures within the vaccuum chamber, and so these results could not be checked independently.
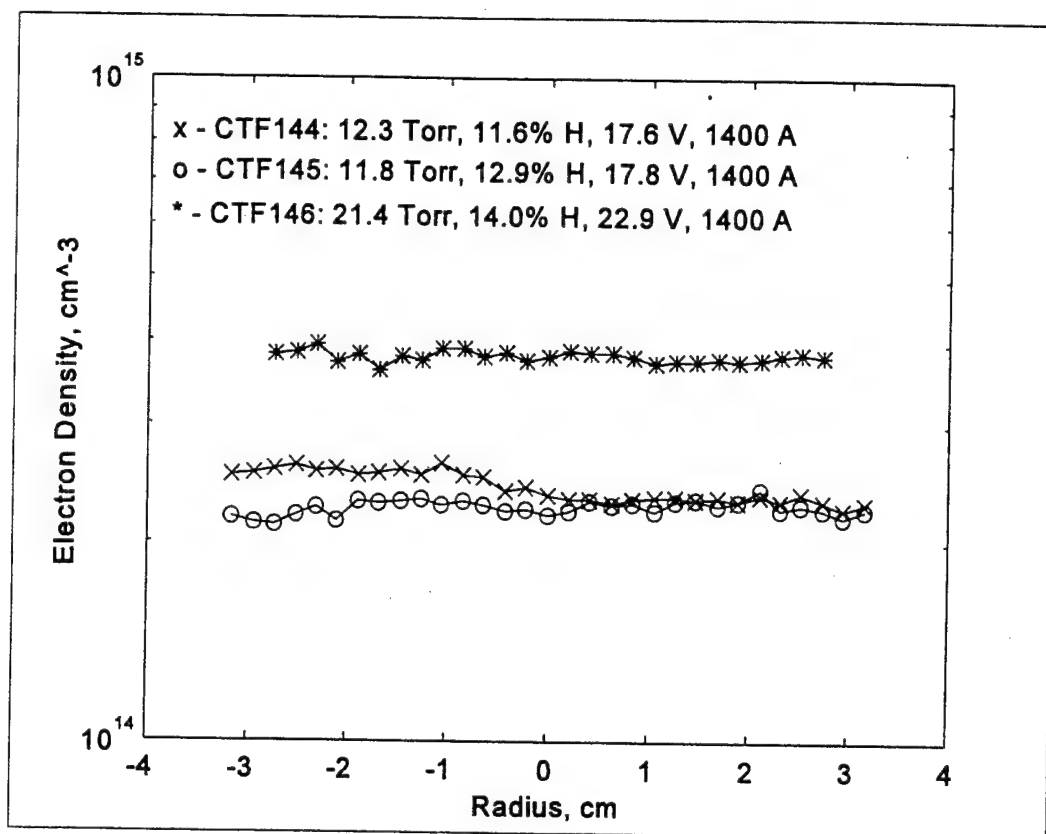
Figure 5.1. Radial Electron Density Profiles Obtined for CTF's 144, 145 and 146 Using the LINBROAD Program. Tank pressure, hydrogen to total volume flow rate, cathode / anode voltage and cathode current are listed for each data set.

Figure 5.2. Radial Electron Temperature Profiles Obtained for CTF's 144, 145 and 146 Using the LINBROAD Program. Tank pressure, hydrogen to total volume flow rate, cathode / anode voltage and cathode current are listed for each data set.

1.   CTF144

Data were first collected for $R \geq 0$. Then, the fiber optic inlet was centered again, and data was collected for $R < 0$. During the collection of the lower half of the data set, operating conditions within the vacuum chamber were observed to change. An increase of hydrogen flow from 0.8 to 1.4 SLPM was observed, along with a major upward shift in the cathode temperature profile near the tip. This shift could be responsible for the slight change in densities and temperatures shown in the region of $-1 < R < 0$ cm in Figure 5.1. It appears as if electron densities and temperatures reached a sort of "steady state" condition towards the end of the recording of the data set. Figure 5.3 below shows the center scan ($R = 0$ cm) from this data set, before being analyzed. Note the two nearby

49

argon lines, one at 4866Å and the other, weaker line beginning to show at around 4856Å. It can be seen that a fair amount of noise is present in the wings of the 4861.33Å hydrogen line, as well as at the line center. The scaling of the intensity into both positive and negative voltage values is also evident. It was this offset that necessitated an "offset constant" be included in the curve fitting programs.
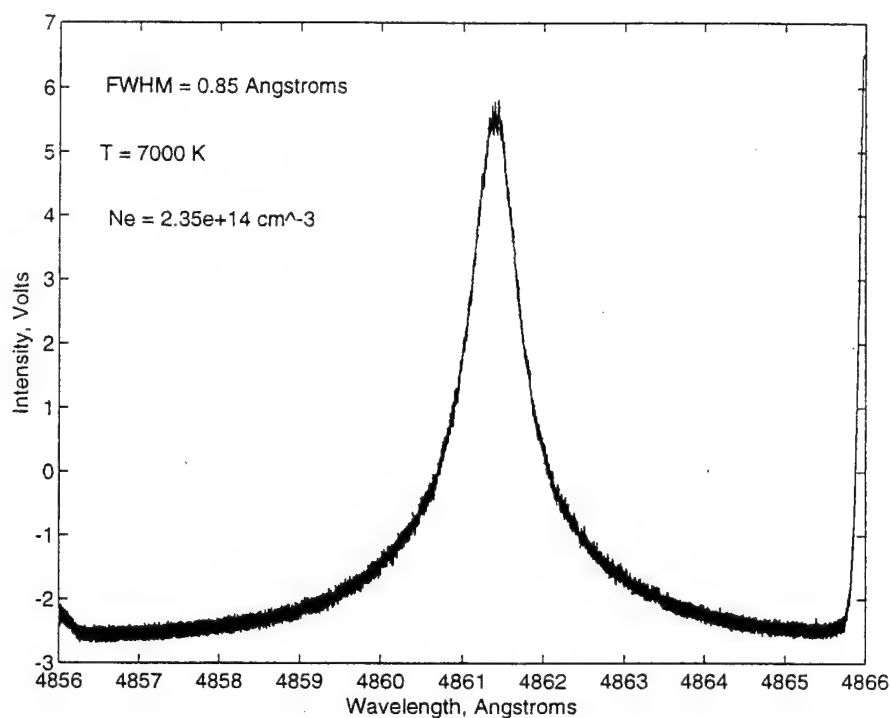
Figure 5.3. CTF144 Center Scan, Raw Data.

2.   CTF145

On the average, the CTF145 lines were narrower than those in CTF144, despite similar operating voltage and current. Hydrogen flow rate was slightly higher than CTF144, with a difference in pressure of -0.5 Torr. No shifts in operating conditions

were observed during the data collection, and again temperature and density behavior is fairly constant throughout the profile. Maximum and minumum density values differ by 12.6%, and density values are between 7 and 8% less than those observed in CTF144. Temperatures are between 16 and 19% less than those of CTF144 as well. The decreased operating pressure during this data collection may contribute to this "falling off" of density and temperature. Being that the cathode jet is a fairly well contained plume of plasma, both by magnetic and tank pressure, it is doubtful that the location of this data set a mere one half inch from the cathode tip would show any major differences in electron densities of temperatures than one taken directly off the cathode tip.

Figure 5.4 shows the center scan for CTF144. The realtive intensity of the accompanying argon lines is noticeably decreased. The higher hydrogen flow rate (12.9% of total vice 11.8%) may partially account for this by increasing the number of hydrogen emitters relative to argon.

FWHM = 0.81 Angstroms

T = 6250 K

Ne = 2.21e+14 cm^-3
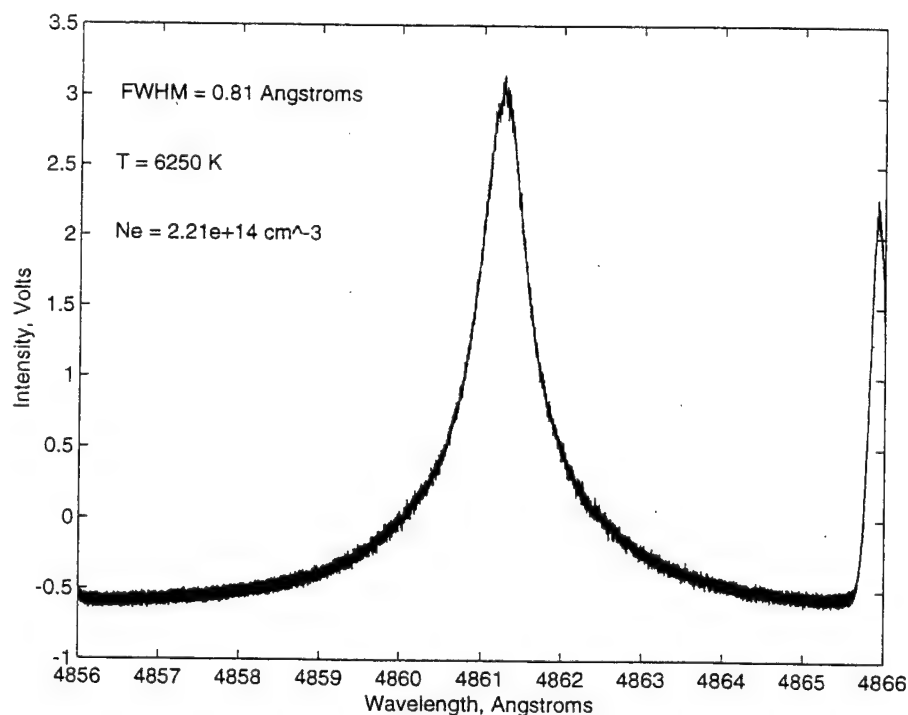
Figure 5.4. CTF145 Center Scan, Raw Data.

3.   CTF146

Scan 30 of CTF146 could not be completely loaded from disk due to a disk error, so the data set was shrunk to 27 data files by eliminating the last two scans on either end of the data set. For this set, tank pressure and voltage were significantly increased, to 21.4 Torr and 22.9 volts respectively. The resulting line profiles are significantly broader, reflecting much higher temperatures and electron densities compared to the other two data sets. Under the increased pressure the electron density distribution is much more uniform, with maximum and minimum values differing by only 9.4%, with no increasing or decreasing trends evident across either the temperature or the pressure profile. With increased power, (*VI*) the hotter cathode is stripping more electrons and generating more ions, while the increased pressure acting on the cathode jet forces the particles in the plume closer together into a denser, more uniform distribution.

The CTF146 center scan, shown in Figure 5.5 is very noticeably broadened, especially in the line wings and the "transition region" between the wings and line center.
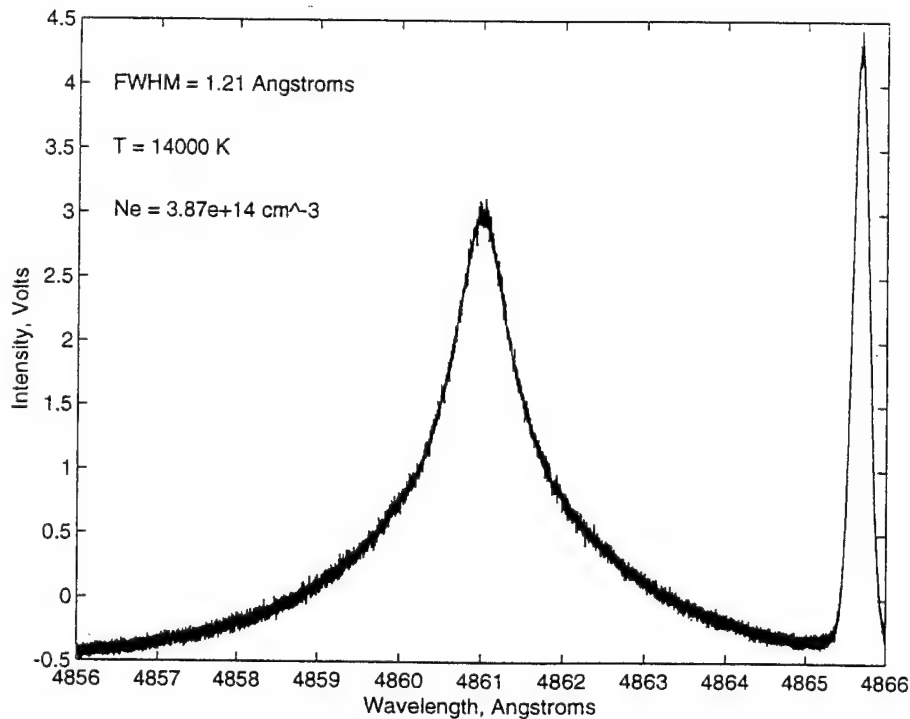
Figure 5.5. CTF146 Center Scan, Raw Data.

D. ANALYSIS COMPLICATIONS

The scaling of the intensity values of the line profiles presented problems in the analyzing of the data, particularly in the fitting routines used to model the data. As is evident in Figures 5.3, 5.4, and 5.5, the voltages representing line intensities are scaled such that the line wings settle out at negative levels. Statistical distributions, by their nature, do not accommodate negative values, and trying to curve fit a Voigt profile to one of these data sets is difficult, requiring the inclusion of an "offset parameter" to estimate the actual (positive) background levels with which the profile merges in the line wings. Attempting to fit the profiles with the LORENTZ function written into the program posed little problem, outside of ambiguities in background intensity levels resulting from the estimation of the offset. However, the VOIGT function inherent to the IDL language ran into problems when attempting to fit profiles stretching into negative voltages, and even with an offset parameter figured into the fit, the initial guesses for fit parameters had to be carefully chosen to keep the routine from producing meaningless output.

Attempting to first offset the data into positive voltages before attempting to fit the data proved to be useless, and no good estimate of background levels could be arrived at outside of the offset parameter generated by curve fitting functions. Though reasonably accurate, the fits generated for the profiles were not as good as expected, and some small amount of accuracy was no doubt sacrificed.

VI. CONCLUSIONS

As stated above, no means of directly measuring electron densities are in place at JPL, and this work can only be considered a first (and so far, only) estimate as to the actual electron densities of plasmas generated in the CTF. The fact that this technique is known to be the most accurate method of non-interfering analysis of plasmas (Huddlestone and Leonard, 1965), however, suggests that the results produced by this program should provide a reasonable estimate of the actual values.

The results of the three data sets agree with what is to be expected. Variations in pressure on the plasma jet produce corresponding variations in particle densities and temperatures; this is particularly evident when comparing CTF146 to the other two data sets. Additionally, the uniform radial electron density distribution agrees with Jahn's (1968) statement that an MPD cathode jet has a generally invariant radial electron distribution.

A.   FUTURE TOPICS

In addition to half width measurement, actual matching of observed line profiles to theoretical Stark profiles is a proven method of particle density determination with an accuracy much greater than half width matching alone (Vidal, Cooper and Smith, 1972). A possible way of doing this would be by taking the Fourier transform of the line profiles and de-convolving them with the known Doppler profile for the plasma. The de-convolved profile could then be matched with known line profiles to achieve an accurate measurement of electron densities. This method requires accurate knowledge of the electron temperature, as well as background intensity levels determined in a manner other than presented in this thesis.

This thesis was limited to three data sets only, which were taken from inside the cathode jet of an MPD test facility. Additional regions of exploration within the plasma jets generated in an MPD thruster could be near the surface of the anode, within the anode jet, in the regions between the two jets, and in the sheath region around the cathode. The latter instance would require a translating instrument with far finer resolution than the

55

micrometer used in this experiment, being that the sheath is on the order of several nanometers thick.

Additionally, a means of direct measurement of electron densities and temperatures in the vacuum chamber should also be explored as a way of providing independent verification for the analysis presented here.

APPENDIX A. CODE

Following is the Interactive Data Language (IDL) code developed to determine the electron densities and temperatures for the data sets taken. It consists of thirteen separate IDL procedures, and is run by making a call in IDL to a single procedure called LINBROAD, called as such:

LINBROAD,'<filename>', dx,fwhm,dr,lr,dw,lw,Te,N

Table A.1 defines the parameters as listed in the above statement:

Parameter	Definition
<filename>	Destination file for results.
dx	Radial position of scan, in mm
fwhm	Full half width of data
dr	Ratio of Doppler half width to full half width
dl	Ratio of Lorentzian half width to full half width
dw	Doppler width, in angstroms
lw	Lorentzian width, in angstroms
Te	Electron temperature, in K
N	Electron density, in cm-^{3}

Table A.1. Definition of Input/Output Parameters for IDL Code.

The names of the parameters are entirely up to the user, within the restrictions of filename size and restricted keywords for the IDL language.

```
; LINBROAD
; Master procedure for analysis of broadened 486.133 nm hydrogen line

; Input Variables:

;        ctfno   Name of output file for data storage

;Output Variables:

;        dx      Position of scan (mm)
;        fw      full half-width of line
;        dr      Ratio of Doppler half width to observed half width (full)
;        lr      Ratio of Lorentzian half width to observed half width (full)
;        dw      Doppler width, angstroms
;        lw      Lorentzian (Stark) width, angstroms
;        Te      Electron temperature, K
;        N       Electron density, cm^-3

pro linbroad,ctfno,dx,fw,dr,lr,dw,lw,Te,N

fitfile,lr,dr,fw,dw,lw,dx                    ;Call procedure FITFILE

NeTe,fw,lw,dw,Te,N                           ;Call procedure NETE

storit,ctfno,dx,fw,dr,lr,dw,lw,Te,N          ;Call procedure STORIT

return                                       ;Return

end                                          ;End procedure

@fitfile                                     ;Compile FITFILE
@NeTe                                        ;Compile NETE
@storit                                      ;Compile STORIT
```

```
; FITFILE

; Procedure sequentially reads in 'scan1' through 'scan31', preps and centers data, and
; determines the Doppler and Stark widths of each observed line profile.

;Output Variables

;        lr      Ratio of Lorentzian half width to observed (full) half width
;        dr      Ratio of Doppler half width to observed (full) half width
;        fw      Full half width of observed profile, angstroms
;        dw      Doppler width of observed profile, angstroms
;        lw      Lorentzian (Stark) width of observed profile, angstroms
;        dx      Position of scan (mm)

pro fitfile,lr,dr,fw,dw,lw,dx

  junk = check_math(0,0)

fw = dblarr(31)                          ;Define output arrays fw, dw, lw, lr, dr
dw = fw
lw = fw
lr = lw
dr = lr

dx = (findgen(30) - 15)*0.083*2.54       ;Generate dx

for m = 0,30 do begin

case 1 of                                ;Determine scan to read

(mlt15):  filename = strcompress('scan'+string(31-m),/remove_all)
    else : filename = strcompress('scan'+string(m-14),/remove_all)

endcase

getfile,filename,wl,int,par,lfit         ;Call procedure GETFILE
delta = sqrt(par(3))                     ;Initial Doppler width estimate (half width of
                                         ;Lorentzian fit performed in GETFILE
lint = int-par(0)                        ;Adjust scan and fit for offset determined in
                                         GETFILE

lfit = lfit-par(0)
```

59

```
a= fltarr(4)                                    ;Define  initial-guess  array  for  Voigt
                                                 parameters
a(0) = lint(1500)                               ;          Peak intensity
a(1) = 2.75                                     ;          Damping parameter
a(2) = -delta                                   ;          Doppler width
a(3) = -par(0)                                  ;          Offset parameter

b = a                                           ;Store initial guesses

w = fltarr(n_elements(wl))+1                     ;Define weight vector (no weighting)

chsq = 999                                      ;Set Chi-Squared to 999
chsqp = 1001                                    ;Define previous Chi-Squared value at 1001

vfit = dblarr(3000)                             ;Define array to store fit of Voigt profile

while chsq lt chsqp do begin                    ;Execute loop until Chi-Square minimized

 chsqp = chsq                                   ;Update chisqp
 pre = a(2)                                     ;Store current Doppler width
 vpre = vfit                                    ;Store current fit

vfit = curvefit(wl,int,w,a,function_name = 'voigt_a',/noderivative)   ;Fit Voigt profile

 vint = int + a(3)                              ;Adjust intensity by offset from fit
 vfit = vfit + a(3)                             ;Adjust fit
 dop = a(2)                                     ;Store Doppler width
 chsq = total((vint-vfit)^2/vfit)              ;Compute Chi-Squared of fit

 a = b                                          ;Reset a with initial values, using Doppler
 a(2) = dop                                     ;width from last fit

endwhile                                        ;Re-execute fit

vfit = vpre                                     ;Best fit

halfwidth,wl,vfit,del,ind                       ;Call procedure HALFWIDTH

getpar,pre,del,damp,l,d                         ;Call procedure GETPAR

lr(m) = l                                       ;Lorentz width fraction
```

```
    dr(m) = d                                ;Doppler width fraction


    prowidth,wl,lint,fwhm                    ;Call procedure PROWIDTH
    dw(m) = d*fwhm                           ;Doppler width
    lw(m) = l*fwhm                           ;Lorentzian (Stark) width
    fw(m) = fwhm                             ;Full half width

print,[dw(m),lw(m),fw(m)]

endfor

return                                       ;Return

end                                          ;End

@getfile                                     ;Compile called procedures
@getdata
@voigt_a
@halfwidth
@prowidth
```

```
; GETFILE

; Reads appropriate scan, and fits an initial Lorentzian profile to determine line center and
; provide initial estimate parameters for fitting a Voigt profile.

;Input Variables

;        filename        Name of scan to be read

;Output Variables

;        lam             Wavelength vector, angstroms
;        int             Intensity vector, volts
;        par             Lorentzian fit parameters
;        fit             Lorentzian fitted profile

pro getfile,filename,lam,int,par,fit

wl1=dblarr(5000)                         ;Define arrays for raw data
int1=wl1
wl0=wl1(0)                               ;Set input variables for reading data
int0=int1(0)
wl=dblarr(4600)                          ;wl = wavelength
val=wl                                   ;val = voltage
st="                                     ;Blank string

openr,1,filename                         ;Open input file

for j=0,5 do readf,1,st                  ;Skip first six lines

for j=0,4999 do begin                    ;Read in 5000 point wavelength and voltage
                                         vectors
readf,1,wl0,int0
wl1(j)=wl0
int1(j)=int0
endfor
close,1                                  ;Close input file

wl=wl1(200:4799)                         ;Delete first and last 200 points

val=int1(200:4799)

profcor,wl,val,lam1,int1,coef,fit1       ;Call procedure PROFCOR
```

```
low = where(lam1 lt coef(2)-3.0,locount)      ;Set cutoff at +/- 3 angstroms from line center

high = where(lam1 gt coef(2)+3.0,hicount)
locut = locount
hicut = n_elements(lam1)-hicount

lam = extrac(lam1,locut,hicut-locut)          ;Extract working vectors from withing cutoffs
int = extrac(int1,locut,hicut-locut)
fit = extrac(fit1,locut,hicut-locut)
par = coef                                    ;Parameters from Lorentzian fit

dl = abs(lam(0:1499) - coef(2))               ;Split profile into left and right sides
dr = lam(1499:2999) - coef(2)
x = sort(dl)
lint = int(x(*))                              ;"Flip" left hand array
rint = int(1499:2999)
hint = (lint+rint)/2                          ;Average left and right hand arrays

int(0:1499) = hint(x(*))                      ;"Unflip" left hand array
int(1500:2999) = hint

return                                        ;Return
end                                           ;End

@profcor                                      ;Compile called procedures
```

63

```
; PROFCOR

; Fit initial Lorentzian profile to data

;Input Variables

;        lam_0           Wavelength
;        int_0           Intensity

;Output Variables

;        lam             Centered wavelength
;        int             Returned intensity
;        coeff           Fit coefficients
;        yfit            Fit

pro profcor,lam_0,int_0,lam,int,coeff,yfit

   ain = [-1.0,7.0,4861.33,0.2]              ;Initial parameter guess

   lorfit,lam_0,int_0,ain,yfit,a            ;Call procedure LORFIT
   lam = lam_0 - a(2)+4861.33               ;Set center wavelength to 4861.33 angstroms

   lorfit,lam,int_0,ain,yfit,a             ;Fit around 4861.33 angstroms

   int = int_0

coeff = a

return                                      ;Return

end                                         ;End

@lorfit                                     ;Compile called procedures
```

```
; LORFIT

; Fits user-defined Lorentzian function

;Input Variables

;       x              X vector
;       y              Y vector
;       ain            Initial parameter guess

;Output Variables

;       yfit           Fitted Lorentzian
;       aout           Returned parameter vector
;       sigma_a        Standard deviation vector

pro lorfit,x,y,ain,yfit,aout,sigma_a

   w = fltarr(n_elements(x))+1              ;Define weight vector (no weighting)

   aout = ain

   yfit = curvefit(x,y,w,aout,sigma_a,function_name = 'lorentz')        ;Perform fit


   return                                   ;Return

end                                         ;End

@lorentz                                    ;Compile fitted function
```

```
; LORENTZ

;Defines Lorentzian function

;Input Variables

;       x               X vector
;       a               Parameters (constants)

;Output Variables

;       f               Returned function
;       pder            Array of partial derivatives wrt parameters

pro lorentz,x,a,f,pder

    f = a(0) + a(1) / ((x - a(2))^2 + a(3))          ;Define Lorentzian function

    if n_params() ge 4 then begin                    ;Define partial derivatives

      pder = fltarr(n_elements(x),4)

      pder(*,0) =  1.0

      pder(*,1) =  1.0/((x-a(2))^2+a(3))

      pder(*,2) =  2*a(1)*(x-a(2))/((x-a(2))^2+a(3))^2

      pder(*,3) =  -a(1)/((x-a(2))^2+a(3))^2

    endif

end                                                   ;End
```

```
; VOIGT_A

;Define Voigt function for curve fitting based on the IDL "Voigt" function

;Input Variables

;      lam           Wavelength
;      a             Fit parameters

;Output Variables

;      f             Returned function
;      pder          Partial derivative vector (not used)

pro voigt_a,lam,a,f,pder

  u = (lam - 4861.33)/a(2)           ;Dimensionless wavelength vector
  f = a(0)*voigt(a(1),u) - a(3)      ;Voigt function

return                                ;Return

end                                   ;End
```

```
;HALFWIDTH

; Determines full half width of Voigt profile

;Input Variables

;       lam            Wavelength
;       v              Voigt function

;Output Variables

;       hw             Half width of profile, in angstroms
;       a              Index of half maximum point

pro halfwidth,lam,v,hw,a

  val = abs((max(v)/2-v)/(max(v)/2))        ;Determine half max value
  a = where(val eq min(val))                ;Locate half max

  hw = abs(lam(1499) - lam(a))              ;Half width

return                                      ;Return

end                                         ;End
```

```
;GETPAR

;Determines damping ratio, Lorentzian and Doppler fractional half widths given doppler
width
;and half width of Voigt profile.

;Input Variables

;       dw              Doppler width
;       hw              Half width

Output Variables

;       d               Damping parameter
;       lr              Lorentzian fractional half width
;       dr              Doppler fractional half width

pro getpar,dw,hw,d,lr,dr

damp = fltarr(29)                               ;Define input arrays
lco = damp
dco = damp
damp0 = damp(0)                                 ;Define input variables
lco0 = lco(0)
dco0 = dco(0)

openr,1,'voigtdat'                              ;Open input file

for j = 0,28 do begin

  readf,1,damp0,lco0,dco0                       ;Read Voigt parameters
  damp(j) = damp0
  lco(j) = lco0
  dco(j) = dco0

endfor

close,1                                         ;Close input file
```

```
coef = poly_fit(dco,lco,2)              ;Binomial fit of Doppler and Lorentz ratios

dr = abs(dw/hw)                         ;Doppler ratio of voigt profile
lr = coef(0)+coef(1)*dr+coef(2)*dr^2    ;Lorentz Ratio
d = lr/dr                               ;Damping parameter

return                                  ;Return

end                                     ;End
```

```
;PROWIDTH

; Determines full half width of data.  Profile width computed by averaging data values over
a 20
; point spread, centered about every data point except the first and last ten. Values are then
;compared to the average of the 20 values centered around the line center.

;Input Variables

;       l               Wavelength
;       int             Intensity

;Output Variables

;       fw              Full half width

pro prowidth,l,int,fw

left = l(0:1499)                          ;Split profile into left and right
right = l(1500:2999)
li = int(0:1499)
ri = int(1500:2999)


half = total(int(1489:1509))/42           ;Average 20 points around line center
                                          ;and find half maximum


lcomp = dblarr(1480)                      ;Comparison  arrays  -  percentage
                                          difference
rcomp = lcomp                             ;between  averaged  values  and  half
                                          max


lval = lcomp                              ;Average values of every 20 points in data
                                          (left)
lind = lcomp                              ;Index of point around which average is taken
                                          (left)


rval = lcomp                              ;Average values of every 20 points in data (right)
   rind= lcomp                                    ;Index of point around which average
is taken (right)


for a = 0,1479 do begin                   ;Average 20 points about every point and
                                          record
                                          ;Index of each point averaged
```

71

```
b = a+10

lval(a) = total(li(b-10:b+10))/21
lcomp(a) = abs((lval(a) - half)/half)
lind(a) = b

rval(a) = total(ri(b-10:b+10))/21
rcomp(a) = abs((rval(a) - half)/half)
rind(a) = b

endfor

lx = where(lcomp eq min(lcomp))          ;Compute index closest to half max
                                          (left)
lhw = abs(left(lind(lx)) - 4861.33)      ;Compute half width (left)

rx = where(rcomp eq min(rcomp))          ;Compute index closest to half max
                                          (right)
rhw = abs(right(rind(rx)) - 4861.33)     ;Compute half width (right)

fw = rhw+lhw                              ;Full half width

return                                    ;Return

end                                       ;End
```

```
;NETE

;Computes electron density and temperature

;Input variables

;       fw              Full half width
;       lw              Lorentzian (Stark) width (full)
;       dw              Doppler width (full)

;Output Variables

;       Te              Temperature (K)
;       N               Electron density (cm^-3)

pro NeTe,fw,lw,dw,Te,N

   halfest,fhw,logNe,T,spln                         ;Call procedure HALFEST
   a = n_elements(fw)                               ;Set counting variable
   ln = dblarr(a)                                   ;log(N) vector
   N = ln                                           ;N vector

   d = dw/2                                         ;Half Doppler width
   m = 1.67e-27                                     ;Hydrogen mass
   k = 1.38e-23                                     ;Boltzmann constant
   c = 3e8                                          ;Speed of light
   lam0 = 4861.33                                   ;Center wavelength

   Te = m/(2*alog(2)*k)*(-c*d/lam0)^2               ;Compute electron temperature
   logTe = alog10(Te)                               ;log(Te)

   hwest = fltarr(a,4)                              ;2D array of half width versus log(N)
                                                    ;to be interpolated from fhw

   for j = 0,a-1 do begin                           ;Spline interpolation to determine
                                                    log(N) vs
                                                    ;log(lw) for T

    for i = 0,3 do begin

     hwest(j,i) = spl_interp(alog10(T),fhw(*,i),spln(*,i),logTe(j))

    endfor
```

```
lN(j) = interpol(logNe,alog10(hwest(j,*)),alog10(lw(j)))    ;Linear interpolation of log(N) vs
                                                            ;log(lw) to determine log(N)

endfor

N = 10^lN                                                    ;Electron density

return                                                       ;Return

end                                                          ;End

@halfest                                                     ;Compile
```

```
;HALFEST

;Read in log(N) vs alpha table and generate cubic spline for interpolation of electron density.

;Output Variables

;       hw              Full stark widths (2D array)
;       logN            Log (base 10) of electron density vector
;       T               Electron temperature vector
;       spln            Spline coefficients (2D array)

pro halfest,hw,logN,T,spln

openr,1,'alpha'                                 ;Open input file
logN = fltarr(4)                                ;Define vectors and arrays
T = logN
hw = fltarr(4,4)
spln = hw

b = 2.0/3.0                                      ;Electron density exponent

for i = 0,3 do begin                            ;Fill T vector and half width matrix

  for j = 0,3 do begin

        readf,1,T0,N,a0
        T(i) = T0*1000
        if T0 eq 5 then logN(j) = N
        hw(i,j) = a0*2.5e-9*(10^N)^b

  endfor ;j

endfor   ;i

for i = 0,3 do begin

  spln(*,i) = spl_init(alog10(T),hw(*,i))       ;Generate splines

endfor

close,1                                         ;Close input file
return                                          ;Return
end                                             ;End
```

75

```
;STORIT

;Writes results of analysis to file

;Input Variables

;       filename      File name to write data to
;       dx            Scan position, mm
;       fw            Full half width
;       dr            Doppler fractional width
;       lr            Lorentzian fractional width
;       dw            Doppler width
;       lw            Lorentzian (Stark) width
;       Te            Electron temperature, K
;       N             Electron density, cm^-3

pro storit,filename,dx,fw,dr,lr,dw,lw,Te,N

openw,1,filename                              ;Open write file

for j = 0,30 do begin

printf,1,dx(j),fw(j),dr(j),lr(j),dw(j),lw(j),Te(j),N(j)   ;Write data to file

endfor

close,1                                       ;Close write file

return                                        ;Return

end                                           ;End
```

APPENDIX B. TABULATED RESULTS

On the following pages are, in tabulated format, some of the results from CTF's 144, 145, and 146. Included are radial position, full half width, Doppler and Stark half widths, electron temperature, and both the log and decimal values for the electron density.

R, cm	Half Widths, Angstroms			T, K	logNe	Ne, x10^14 cm^-3
	Full	Doppler	Stark			
-3.1623	0.906	0.3191	0.7827	8463	14.403	2.529298
-2.95148	0.89	0.296	0.7816	7283	14.404	2.5351286
-2.74066	0.894	0.2914	0.7894	7054	14.411	2.5763212
-2.52984	0.914	0.312	0.797	8091	14.415	2.6001596
-2.31902	0.898	0.3012	0.7869	7540	14.408	2.5585859
-2.1082	0.906	0.3068	0.7918	7823	14.411	2.5763212
-1.89738	0.902	0.3157	0.7808	8283	14.402	2.5234808
-1.68656	0.898	0.3069	0.7828	7826	14.404	2.5351286
-1.47574	0.902	0.3043	0.7891	7694	14.41	2.5703958
-1.26492	0.906	0.3217	0.7808	8602	14.401	2.5176769
-1.0541	0.914	0.3042	0.8026	7691	14.42	2.630268
-0.84328	0.898	0.3097	0.7807	7971	14.402	2.5234808
-0.63246	0.89	0.3035	0.7763	7653	14.399	2.5061093
-0.42164	0.85	0.2787	0.7494	6457	14.379	2.3933158
-0.21082	0.858	0.2808	0.7568	6554	14.386	2.432204
0	0.85	0.2894	0.7417	6958	14.372	2.3550493
0.21082	0.842	0.2848	0.7361	6742	14.367	2.3280913
0.42164	0.85	0.2965	0.7365	7305	14.366	2.3227368
0.63246	0.846	0.2974	0.7314	7348	14.362	2.3014418
0.84328	0.842	0.2852	0.7358	6758	14.367	2.3280913
1.0541	0.842	0.282	0.7381	6609	14.369	2.3388372
1.26492	0.846	0.2886	0.7378	6922	14.368	2.3334581
1.47574	0.85	0.2946	0.7379	7214	14.368	2.3334581
1.68656	0.85	0.2917	0.7401	7070	14.37	2.3442288
1.89738	0.846	0.2967	0.7318	7317	14.362	2.3014418
2.1082	0.846	0.2849	0.7405	6744	14.371	2.3496328
2.31902	0.83	0.2738	0.7306	6229	14.363	2.3067472
2.52984	0.846	0.2779	0.7455	6419	14.376	2.3768403
2.74066	0.834	0.2799	0.7307	6511	14.363	2.3067472
2.95148	0.822	0.2777	0.7189	6409	14.353	2.2542392
3.1623	0.83	0.2761	0.7289	6337	14.362	2.3014418

Table B.1. CTF 144 Results

| | Half Widths, Angstroms | | | | | Ne, x10^14 |
R, cm	Full	Doppler	Stark	T, K	logNe	cm^-3
-3.1623	0.798	0.2628	0.7027	5740	14.3405	2.1902818
-2.95148	0.79	0.2659	0.6916	5876	14.33	2.1379621
-2.74066	0.794	0.2732	0.6908	6201	14.3282	2.1291193
-2.52984	0.802	0.2666	0.7047	5907	14.3417	2.1963422
-2.31902	0.814	0.2666	0.7178	5908	14.3536	2.2573557
-2.1082	0.81	0.2874	0.6982	6865	14.3333	2.1542693
-1.89738	0.826	0.2679	0.7303	5963	14.364	2.3120648
-1.68656	0.834	0.2847	0.7272	6735	14.36	2.2908677
-1.47574	0.834	0.2813	0.7297	6575	14.3622	2.3025019
-1.26492	0.846	0.2899	0.7369	6985	14.367	2.3280913
-1.0541	0.834	0.2864	0.7259	6818	14.3583	2.2819178
-0.84328	0.826	0.2674	0.7306	5942	14.3648	2.3163277
-0.63246	0.83	0.2836	0.7235	6686	14.3565	2.2724796
-0.42164	0.822	0.2832	0.7149	6664	14.3489	2.233058
-0.21082	0.822	0.2797	0.7174	6500	14.3516	2.2469841
0	0.81	0.2742	0.7079	6250	14.3438	2.2069881
0.21082	0.822	0.2834	0.7147	6674	14.3487	2.2320299
0.42164	0.822	0.2643	0.7284	5803	14.3632	2.3078097
0.63246	0.834	0.2869	0.7256	6842	14.3579	2.2798171
0.84328	0.83	0.2975	0.7265	6494	14.3596	2.2887587
1.0541	0.818	0.2787	0.7136	6457	14.3483	2.229975
1.26492	0.842	0.2891	0.7329	6946	14.3641	2.3125972
1.47574	0.838	0.2817	0.7339	6595	14.3658	2.3216674
1.68656	0.834	0.2888	0.7242	6931	14.3565	2.2724796
1.89738	0.83	0.2738	0.7306	6230	14.3639	2.3115325
2.1082	0.826	0.2445	0.7461	4966	14.3814	2.4065783
2.31902	0.826	0.283	0.7195	6655	14.353	2.2542392
2.52984	0.826	0.2778	0.7233	6413	14.357	2.2750974
2.74066	0.834	0.2934	0.7208	7153	14.353	2.2542392
2.95148	0.822	0.2931	0.7074	7140	14.341	2.1928049
3.1623	0.826	0.285	0.718	6752	14.3514	2.2459496

Table B.2. CTF 145 Results.

R, cm	Half Widths, Angstroms			T, K	logNe	Ne, x10^14 cm^-3
	Full	Doppler	Stark			
-2.74066	1.194	0.4061	1.042	13707	14.5794	3.7966451
-2.52984	1.206	0.4162	1.048	14393	14.5827	3.8256039
-2.31902	1.234	0.4269	1.072	15145	14.5963	3.9472988
-2.1082	1.174	0.4023	1.022	13457	14.5675	3.6940264
-1.89738	1.206	0.4188	1.046	14577	14.5814	3.8141696
-1.68656	1.154	0.3954	1.005	12995	14.557	3.6057864
-1.47574	1.194	0.4069	1.042	13762	14.579	3.7931498
-1.26492	1.186	0.4107	1.03	14023	14.5716	3.7290654
-1.0541	1.214	0.4137	1.059	14224	14.5892	3.8832916
-0.84328	1.21	0.4078	1.059	13820	14.5894	3.8850803
-0.63246	1.19	0.4066	1.037	13737	14.5765	3.7713775
-0.42164	1.214	0.425	1.051	15013	14.5838	3.8353058
-0.21082	1.202	0.433	1.031	15578	14.5716	3.7290654
0	1.186	0.3981	1.039	13174	14.5778	3.7826835
0.21082	1.21	0.4109	1.057	14033	14.5879	3.8716849
0.42164	1.198	0.4035	1.048	13537	14.5833	3.8308928
0.63246	1.206	0.4133	1.05	14199	14.584	3.8370725
0.84328	1.194	0.4073	1.041	13788	14.5788	3.7914034
1.0541	1.182	0.4133	1.023	14199	14.5676	3.6948771
1.26492	1.182	0.4025	1.031	13462	14.573	3.7411059
1.47574	1.174	0.3941	1.028	12909	14.5716	3.7290654
1.68656	1.186	0.4029	1.036	13491	14.5755	3.7627035
1.89738	1.19	0.416	1.03	14379	14.5718	3.7307831
2.1082	1.194	0.416	1.035	14373	14.5746	3.754914
2.31902	1.198	0.4062	1.046	13713	14.5821	3.8203223
2.52984	1.206	0.4141	1.05	14258	14.5836	3.83354
2.74066	1.198	0.4083	1.045	13852	14.5811	3.8115358

Table B.3. CTF 146 Results

APPENDIX C. DATA TABLES

Two tables are presented here which were used in the analysis program listed in Appendix A. Table C.1, from Huddlestone and Leonard (1965) is a tabulation of Voigt profile characteristics, where λ_D is the Doppler half width, λ_L is the Lorentzian half width, and $\lambda_{1/2}$ is the observed half width of the Voigt profile. The first column, λ_L/λ_D, represents the damping parameter of the profile. The second and third columns display, respectively, the ratios of Lorentzian and Doppler half widths to the profile width. Using columns two and three, a second order polynomial fit of λ_L vs λ_D was generated, from which a value of λ_L could be determined, given λ_D and $\lambda_{1/2}$.

Table C.2 from Griem (1974) lists computed $\alpha_{1/2}$ relative to electron densities and temperatures. These data are interpolated using cubic splines in order to determine the half widths corresponding to each electron density for the value of T_e computed from the Doppler half width of the profile. Once the half widths are determined, a linear interpolation (on a log-log scale) of N_e vs half width is made for the Lorentzian half width of the profile, and an electron density is determined.

λ_I/λ_L	λ_I/λ_L	λ_I/λ_L
∞	1	0
12.01	0.993	0.083
6.01	0.972	0.162
4.00	0.941	0.235
3.00	0.904	0.301
2.70	0.886	0.327
2.40	0.863	0.359
1.80	0.794	0.441
1.50	0.742	0.494
1.20	0.672	0.559
1.14	0.655	0.574
1.08	0.637	0.589
1.02	0.618	0.605
0.96	0.597	0.622
0.90	0.575	0.639
0.84	0.552	0.656
0.78	0.527	0.675
0.72	0.5	0.694
0.66	0.472	0.715
0.60	0.442	0.736
0.54	0.41	0.758
0.48	0.375	0.78
0.42	0.338	0.804
0.36	0.299	0.829
0.30	0.257	0.855
0.24	0.212	0.882
0.18	0.164	0.91
0.12	0.113	0.939
0.05	0.05	0.984
0	0	1

Table C.1. Half widths of Voigt profiles (From Huddlestone and Leonard, 1965)

log(Ne)	14	15	16	17
Electron Density, cm^-3	Full half width, alpha (unitless)			
5000	7.62e-02	7.87e-02	8.08e-02	7.65e-02
10000	7.74e-02	8.03e-02	8.40e-02	8.51e-02
20000	7.77e-02	8.15e-02	8.60e-02	9.02e-02
40000	7.90e-02	8.14e-02	8.61e-02	9.27e-02
	Full half width, angstroms			
5000	0.4104198	1.9675	9.3760094	41.203563
10000	0.4168831	2.0075	9.7473366	45.835598
20000	0.4184989	2.0375	9.979416	48.582502
40000	0.4255009	2.035	9.99102	49.929024

Table C.2. Half width of theoretical Stark profiles vs N_e, T_e. (From Griem, 1974).

LIST OF REFERENCES

Chen, F. F., *Introduction to Plasma Physics*, Plenum Press, 1977.

Cobine, J. D., *Gaseous Conductors*, McGraw-Hill, 1941.

Eisberg, R., Resnick, R., *Quantum Physics of Atoms, Molecules, Solids, Nuclei, and Particles*, John Wiley and Sons, Inc., 1985.

Goodfellow, K., "A Theoretical and Experimental Investigation of Cathode Processes in Electric Thrusters", PhD Dissertation, University of Southern California, Department of Aerospace Engineering, May 1996.

Griem, H., *Plasma Spectroscopy*, McGraw-Hill, 1964.

Griem, H., *Spectral Line Broadening by Plasmas*, Academic Press, 1974.

Herzberg, G., *Atomic Spectra and Atomic Structure*, Dover Publications, 1944.

Hoskins, W., Kull, A., Butler, G., *Measurement of Population and Temperature Profiles in an Arcjet Plume*, AIAA, 1992.

Jahn, R., *Physics of Electric Propulsion*, McGraw-Hill, 1968.

Huddlestone, R., Leonard, S., *Plasma Diagnostic Techniques*, Academic Press, 1965.

Marr, G., *Plasma Spectroscopy*, Elsevier, 1968.

Sutton, G., *Rocket Propulsion Elements*, John Wiley and Sons, 1992.

Vidal, C., Cooper, J., Smith, E., "Hydrogen Stark Broadening Calculations with the Unified Classical Path Theory", Journal of Quantitative Spectroscopy and Radiative Transfer, vol 10, 1970.

Vidal, C., Cooper, J., Smith, E., "Unified Theory Calculations of Stark Broadened Hydrogen Lines Including Lower State Interactions", NBS Monograph 120, National Bureau of Standards, 1971.

Vidal, C., Cooper, J., Smith, E., "Hydrogen Stark Broadening Tables", The Astrophysical Journal Supplement Series, no. 214, vol 10, 1973.

Von Engel, A., *Ionized Gases*, Oxford, 1965.

86

INITIAL DISTRIBUTION LIST

1. Defense Technical Information Center 2
   8725 John J. Kingman Rd., STE 0994
   Ft Belvoir, Virginia, 22060-6218

2. Dudley Knox Library 2
   Naval Postgraduate School
   411 Dyer Rd.
   Monterey, California, 93943-5101

3. Professor David Cleary 1
   PH/Cl
   Naval Postgraduate School
   Monterey, California, 93943

4. Professor Oscar Biblarz 1
   AA/Bi
   Naval Postgraduate School
   Monterey, California, 93943

5. Dr. John Brophy 1
   Advanced Propulsion Technology Group
   NASA JPL
   4800 Oak Grove Dr.
   Pasadena, California, 91109
   M/S 125-224

6. Dr. Keith Goodfellow 1
   Advanced Propulsion Technology Group
   NASA JPL
   4800 Oak Grove Dr.
   Pasadena, California, 91109
   M/S 125-224

7. LT Briget Horner, USN 1
   Code 37
   Naval Postgraduate School
   Monterey, California, 93943